nature communications

Article

https://doi.org/10.1038/s41467-025-63750-2

Platelet activation plays a pro-inflammatory role in myasthenia gravis

Received: 13 June 2024

Accepted: 27 August 2025

Published online: 02 October 2025

Check for updates

Qi Wen[1,5,6,7], Shu Zhang[1,7], Yaye Wang[1,7], Haoran Liu[1,7], Jingsi Wang[1], Shengyao Su[1], Nairong Xie[1], Yan Lu[1], Li Di[1], Min Xu[1], Min Wang[1], Hai Chen[1], Suobin Wang[1], Wenjia Zhu[1], Xinmei Wen[1], Jinming Han[2], Dongshan Wan[2], Shufang Zhao[2], Wanting Lu[2], Zhen Tao[3], Jianying Duo[1], Yue Huang[1], Guoliang Chai[2], Ruisheng Duan[4], Xiaoli Li[4,8] ✉, Junwei Hao[2,8] ✉ & Yuwei Da[1,8] ✉

Myasthenia gravis (MG) is an autoimmune disorder that disrupts neuromuscular junction function through autoantibodies. Platelets are emerging as key players in the pathogenesis of MG, bridging innate and adaptive immunity. We analyze platelet transcriptome signatures and their interactions with the immune system in AChR+ immunotherapy-naïve MG (nMG) patients using bulk and single-cell RNA sequencing on peripheral blood mononuclear cells (PBMC). nMG patients exhibit upregulation of genes related to activation, inflammation, and cytoskeletal regulation. Increased platelet count, activation, altered morphology, enhanced CD62P expression, and elevated plasma CD40L levels are observed in PBMCs, which diminish with minimal clinical status (MMS). Functionally, platelets show heightened interactions with leukocytes, forming aggregates that correlate with disease severity. These features return to baseline after intravenous immunoglobulin or prolonged immunosuppressive therapy. This study underscores platelet activation's critical role in MG and supports platelet-targeted therapy.

Myasthenia gravis (MG) is an autoimmune disease characterized by the presence of autoantibodies, predominantly acetylcholine receptor antibodies (anti-AChR), in 80%–85% of patients. These antibodies target functional molecules in the postsynaptic membrane, leading to signal transmission impairment and diverse clinical symptoms, including ptosis, dysphagia, limb weakness, and dyspnea[1]. While the disease's pathophysiology is well-established, the underlying mechanisms driving the autoimmune response in MG remain incompletely understood. Dysregulation of CD4+ T cell subtypes, particularly the imbalance of T helper (Th) cells and regulatory T cells (Treg), contributes to the aberrant immune response in MG[2,3]. Chronic inflammation, a key initiator of Th cell imbalance, is believed to stem from innate immunity activation, driving Th cell differentiation and initiating adaptive immunity, with crucial roles played by innate immune cells like dendritic cells and macrophages[4,5].

Platelets, traditionally acknowledged for their role in primary hemostasis, have now emerged as integral players in the innate immune system[6–8]. Their involvement extends to the modulation of CD4+ T cell immune responses[9–11], aiding in T cell adhesion and recruitment[12,13], as well as influencing the differentiation and activation

[1]Department of Neurology, Xuanwu Hospital, Capital Medical University, Beijing, China. [2]Department of Neurology, Xuanwu Hospital, National Center for Neurological Disorders, Capital Medical University, Beijing, China. [3]Institute of Cerebrovascular Disease Research and Department of Neurology, Xuanwu Hospital, Capital Medical University, Beijing, China. [4]Department of Neurology, The First Affiliated Hospital of Shandong First Medical University & Shandong Provincial Qianfoshan Hospital, Jinan, Shandong, China. [5]Present address: Department of Neurology, First Hospital of Shanxi Medical University, Taiyuan, China. [6]Present address: Research Center for Neurological Diseases, Shanxi Medical University, Taiyuan, China. [7]These authors contributed equally: Qi Wen, Shu Zhang, Yaye Wang, Haoran Liu. [8]These authors jointly supervised this work: Xiaoli Li, Junwei Hao, Yuwei Da. ✉e-mail: li2006xl@163.com; haojunwei@vip.163.com; dayuwei100@hotmail.com

of CD4+ T effector cells through a variety of mediators[11,14]. Notably, platelets have been observed to consistently augment Treg cell responses while exerting biphasic effects on Th1 and Th17 activation[15]. The release of soluble factors and expression of surface glycoproteins by activated platelets play a significant role in modulating the functions of immune cells[6]. Critical activation markers, notably P-selectin (CD62P) and CD40 ligand (CD40L/CD154), are instrumental in fostering interactions with leukocytes, thereby contributing to the perpetuation of immune-mediated inflammation[16,17]. In autoimmune disorders like systemic lupus erythematosus (SLE), heightened platelet activation is associated with increased disease severity, where these platelets form complexes with neutrophils and antigen-presenting cells (APCs), including monocytes and plasmacytoid dendritic cells[6,18]. Furthermore, platelet binding to neutrophils alters their phenotype, inducing neutrophil activation and the formation of neutrophil extracellular traps (NETosis), a process linked to the release of autoantigens that are processed by APCs[6]. In certain disease states, changes in platelet number and function are closely associated with NET formation[19,20]. Overall, platelets play multifaceted roles in promoting disease activity in autoimmune disorders.

Huang et al.[21] demonstrated marked elevations in the platelet-lymphocyte ratio (PLR) and systemic immune-inflammation index (SII) among MG patients, with these markers being notably increased in generalized MG (GMG). These elevated indices suggest an intensified release of platelets into the circulation, potentially contributing to the maintenance and exacerbation of systemic autoimmune inflammation[22]. Despite the emerging correlation, the precise role of platelets within MG's pathogenic framework remains largely unknown. Given their involvement in bridging innate and adaptive immune responses, further investigation into the function of platelets in MG may help improve our understanding of disease mechanisms and support the development of potential therapeutic strategies.

In this study, we investigate the activation profile of platelets in AChR+ immunotherapy-naïve MG (nMG) and their interactions with neutrophils and CD4+ T cells by integrating transcriptomic and functional analyses. Our findings reveal that nMG platelets exhibit a distinct pro-inflammatory phenotype, driving NETs formation, which in turn amplifies platelet activation, establishing a reciprocal activation loop. Additionally, nMG platelets modulate CD4+ T cell responses by enhancing Th1 cytokine production and suppressing Treg differentiation. These findings highlight the role of platelets in immune dysregulation in MG and suggest potential therapeutic avenues for targeted intervention.

Results

Single-cell survey and laboratory data show an elevated platelets count in MG

We procure PBMCs from 6 eligible individuals and subsequently perform scRNA-seq using the 10X Genomics platform (Fig. 1). A Schematic overview of the sequencing workflow is presented in Fig. 2a. Post quality control, a total of 88,942 single cells (an average of 11,118 cells per sample) are analyzed. We partition the single-cell profiles into 16 distinct immune cell lineages based on canonical lineage markers and cluster-specific gene expression, and visualize using Uniform Manifold Approximation and Projection (UMAP) (Fig. 2b). The proportional distribution of each cell population across samples is presented in Fig. 2c.

The small population of platelets, present after isolating PBMC preparations, attracts our interest because of their notable expansion in MG patients (Fig. 2d). These platelets are characterized by a set of marker genes, including *PPBP*, *TUBB1*, *PF4*, *CAVIN2*, *NRGN*, *HIST1H2AC*, *GNG11*, *GP9*, *SPARC*, *RGS18*, *CLU*, *TSC22D1*, and *MPIG6B*. Cell proportion analysis reveals a disproportionate augmentation of platelets in MG participants, particularly notable in nMG patients with a higher quantitative myasthenia gravis (QMG) score (nMG3). Platelets comprise 6.82% of the total PBMCs in nMG, compared to 2.53% in healthy control (HC), and 2.16% in patients reaching minimal clinical status (MMS)[23] (Fig. 2e). Notably, the platelet counts decrease in the same patients after achieving MMS, although this reduction does not reach statistical significance ($p = 0.12$). Additionally, there was an upsurge in the expression of genes related to platelet degranulation in nMG patients' PBMCs, which reverses post-treatment (Fig. 2f).

Given that the first three nMG cases are young to middle-aged females, we include an additional elderly male MG patient (nMG4) to investigate whether the observed increase in platelet count is also present in male patients and to assess any potential influence of sex or age on this phenomenon. The QMG score of nMG4 is comparable to that of nMG3. However, due to the absence of matched male HC and post-MMS samples for nMG4, these data are excluded from the primary single-cell analysis to minimize potential bias. Instead, we perform scRNA-seq on PBMCs from this patient and observe that nMG4 also exhibited an increased platelet count along with elevated expression of platelet degranulation genes (Supplementary Fig. 1). These findings indicate that the observed platelet count increase and associated gene expression changes are independent of age and sex, further validating the consistency of this phenomenon. The clinical characteristics, platelet count, and percentage of platelets in PBMCs for each patient are provided in Supplementary Tables 1 and 2 in the Supplementary Materials.

Considering the limited sample size of scRNA-seq and the relatively low number of platelets in PBMCs, along with the significant clinical heterogeneity among nMG patients, we examine peripheral blood platelet counts across a larger cohort with various MG subtypes. This cohort includes 65 nGMG (immunotherapy-naïve GMG), 25 nOMG (immunotherapy-naïve OMG), 40 MMS patients, and 25 HC, with demographic characteristics provided in Supplementary Table 3. The analysis reveals that nGMG patients have elevated platelet counts compared to MMS patients ($p < 0.001$), implying a potential correlation between platelet quantity and MG disease activity (Fig. 2g). Additionally, platelet-related inflammatory markers, such as the SII and PLR, also show corresponding elevations in nGMG patients (Supplementary Fig. 2a, b).

This CellChat network analysis identifies CD8 CTLs (cytotoxic T cells, orange) and CD14 MCs (monocytes, red) as key target cells of platelet-mediated interactions, exhibiting substantial communication activity across all conditions. Notably, the MG and MMS groups demonstrate heightened intercellular communication compared to HC, suggesting a potential immune activation signature in disease states (Fig. 2h). Platelets receive signals primarily from CD8 CTLs, monocytes (CD14 MC, CD16 MC), and dendritic cells (pDCs, cDCs). Among these interactions, ITGB2–CD226 and CD40LG–(ITGA2B +ITGB3) are particularly enriched across multiple immune cell types (Fig. 2i), suggesting their involvement in platelet activation and immune modulation. Conversely, platelets predominantly signal toward CD8 CTLs, engaging in interactions such as HLA-E-CD94/NKG2A, HLA-E-CD8A, and multiple HLA class I molecules binding to CD8B (Fig. 2j), highlighting their potential role in CD8 T cell regulation. Additionally, JAM1-(ITGA4+ITGB2) and ITGB2–CD226 interactions further emphasize platelet-mediated immune cell adhesion and activation. Moreover, strong interactions with monocytes and dendritic cells, including PF4-CXCR3 and PECAM1-PECAM1, suggest a role for platelets in immune recruitment and inflammatory responses (Fig. 2j).

Bulk RNA sequencing reveals a distinct pro-inflammatory transcriptional signature in nMG platelets

To further characterize platelet-associated transcriptional alterations in MG, bulk RNA sequencing is performed on washed platelets from three nMG patients and three age- and sex-matched HC. Clinical

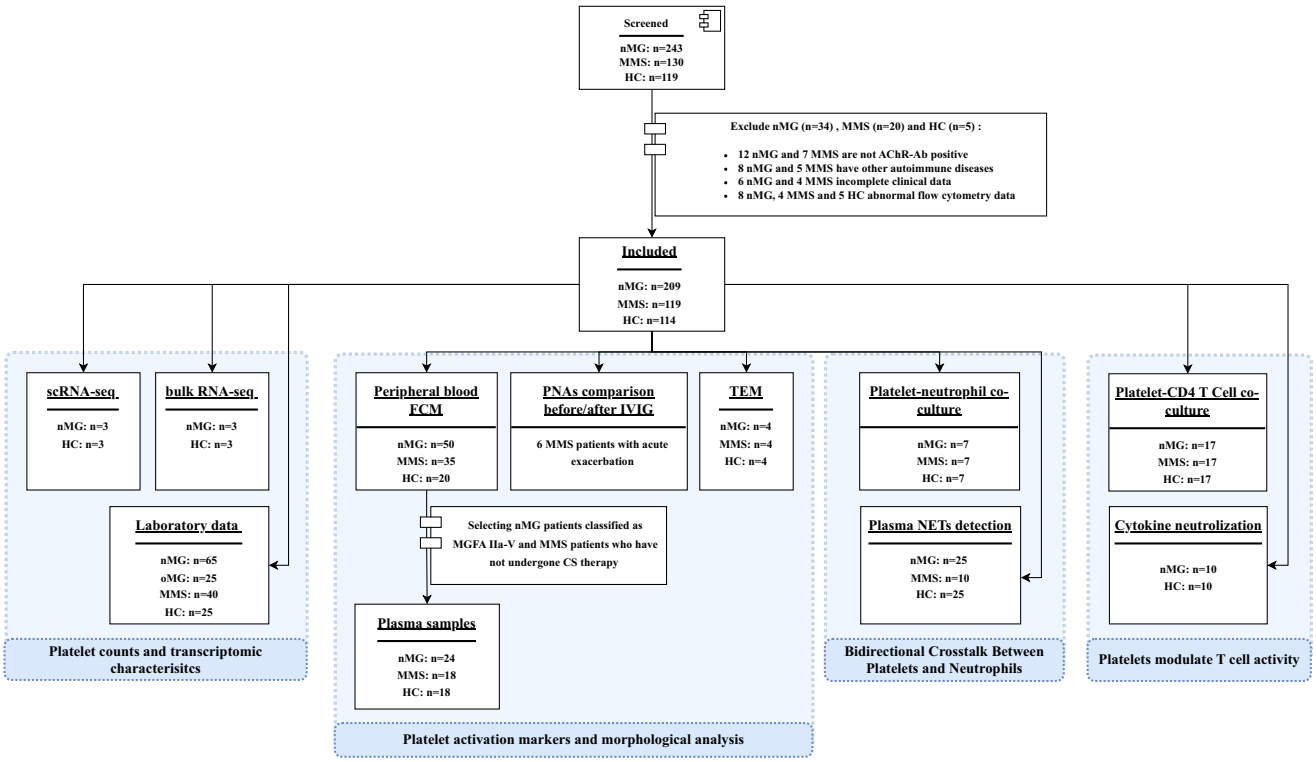

Fig. 1 | Flow chart of participants screening and enrollment in different study parts. nMG immunotherapy-naïve myasthenia gravis, HC healthy controls, MMS minimal clinical status, scRNA-seq single-cell RNA sequencing, TEM transmission electron microscopy, NETs neutrophil extracellular traps.

characteristics of the samples included are detailed in Supplementary Table 4.

A total of 189 upregulated and 250 downregulated differentially expressed genes (DEGs) were identified in nMG platelets compared to HCs (Fig. 3a). GO analysis (Fig. 3b) reveals significant enrichment in immune response modulation and phagocytosis. Pathways related to Fc-gamma receptor signaling and heterotypic cell-cell adhesion are prominently upregulated, indicating hyperactivation of immune effector functions in MG. Additionally, upregulated genes are associated with granule membranes (ficolin-1-rich granules, tertiary granules), lysosomal and phagocytic vesicles, and focal adhesion sites, suggesting increased immune cell activity and intracellular trafficking. Enrichment in actin binding, integrin binding, and antigen binding highlights enhanced immune cell motility, adhesion, and antigen recognition, while upregulated ATPase-coupled transmembrane transport pathways reflect metabolic and signaling alterations in immune processes. KEGG pathway analysis (Fig. 3c) identifies key alterations in immune regulation and metabolic homeostasis. Enriched pathways, including primary immunodeficiency and Fc-epsilon RI signaling, point to dysregulated immune activation in MG pathogenesis. Metabolic pathways, such as the pentose phosphate pathway, fructose and mannose metabolism, and glyoxylate/dicarboxylate metabolism, are also significantly enriched, indicating metabolic reprogramming that may contribute to platelet dysfunction and immune activation. Gene Set Enrichment Analysis (GSEA) (Fig. 3d) further emphasizes immune activation in MG platelets. Key enriched pathways include Fc receptor-mediated signaling (e.g., Fc-gamma and Fc-epsilon receptor pathways), phagocytosis, and membrane invagination, all of which point to enhanced antibody-dependent cellular responses, immune effector activation, and vesicular trafficking. Upregulated endocytosis-related pathways suggest increased antigen uptake and modulation of immune signaling, potentially influencing inflammatory responses in MG. Transcription factor (TF) analysis (Fig. 3e) reveals a distinct regulatory landscape in nMG platelets. The zf-C2H2 family is significantly downregulated, while the bZIP and bHLH families are predominantly upregulated. Notably, STAT, ETS, and THR-like TF families, though less abundant, are implicated in immune signaling, suggesting their role in regulating immune cell differentiation and activation.

These transcriptomic findings indicate a profound shift in platelet function in MG, characterized by heightened immune activation, metabolic reprogramming, and altered transcriptional regulation. While these results suggest a potential role for platelet dysregulation in MG pathophysiology, further studies are needed to validate functional consequences at the protein level and elucidate their direct contributions to disease progression.

Enhanced CD62P expression, sCD40L release, and morphological alterations in MG platelets

To further elucidate the over-activated status of platelets in MG patients at the protein level, we utilize peripheral blood flow cytometry to assess the surface expression of CD62P on platelets and conduct cytokine assays to measure plasma levels of soluble CD40 ligand (sCD40L). Clinical information for the included samples is provided in Supplementary Tables 5 and 6. The gating strategy for CD62P+ platelets is shown in Fig. 4a. The results demonstrate that the proportion of CD62P+ platelets in nMG patients ($n = 50$) is significantly elevated compared to the HC group (HC, $n = 20$; $p = 0.0307$) and MMS group (MMS, $n = 35$; $p = 0.0037$) (Fig. 4b). Additionally, the plasma sCD40L concentration in nMG patients ($n = 24$) (Fig. 4c) is significantly higher than that in the HC group (HC, $n = 18$; $p = 0.0199$). A significant positive correlation is observed between plasma sCD40L levels and QMG score ($n = 24$, $R = 0.57$, $p = 0.0034$) (Fig. 4d). These findings indicate a chronic state of platelet activation in MG patients, which is associated with disease activity. Within the MG cohort, the proportion of CD62P-positive platelets does not show statistical significance ($p = 0.216$) between patients who underwent antiplatelet therapy (APT) and those who

https://doi.org/10.1038/s41467-025-63750-2

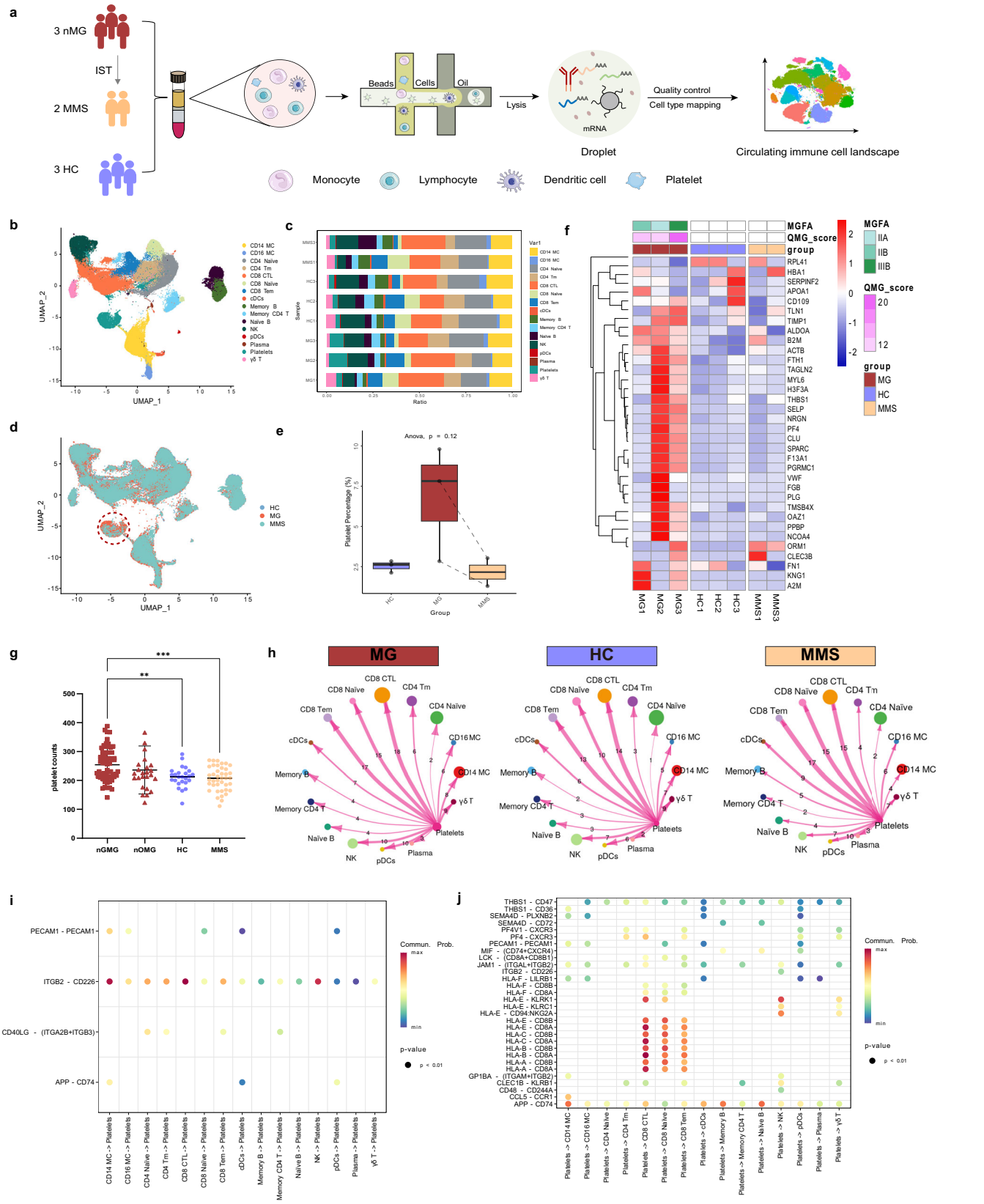

did not, although the former group has a relatively lower mean value (Fig. 4e). Stratification based on disease duration within the nMG and MMS groups reveals that patients with a disease duration greater than 60 months have a lower proportion of activated platelets, but there are no significant differences compared to patients in the other two duration categories (Supplementary Fig. 3a, b). There was also no significant difference in the proportion of CD62P-positive platelets between different gender subgroups (Supplementary Fig. 3c).

Previous studies indicate that platelet volume decreases upon activation compared to the resting state[24], likely due to the release of platelet granule contents as platelet-derived microparticles (PMPs) during the activation process[25]. In flow cytometry detection, different

https://doi.org/10.1038/s41467-025-63750-2

Fig. 2 | PBMCs scRNA-seq revealed elevated platelet count in MG and validated by peripheral blood laboratory test. a Overview of the scRNA-seq experiment: PBMCs were isolated from three HC and three nMG patients, plus samples from two of the aforementioned MG patients when they achieved MMS post-treatment. **b** UMAP representation of scRNA-seq data illustrating the 16 cell types, including CD8+ T cells (CD8 CTL), CD4+ effector T cells (CD4 Tm), natural killer cells (NK), naïve B cells (Naïve B), CD8+ effector memory T cells (CD8 Tem), naïve CD8+ T cells (CD8 Naïve), gamma delta T Cells (γδ T), naïve CD4+ T cells (CD4 Naïve), CD14+ monocytes (CD14 MC), memory B Cells (Memory B), platelets, memory CD4+ T cells (Memory CD4 T), conventional dendritic cells (cDCs), plasmacytoid dendritic cells (pDCs), CD16+ monocytes (CD16 MC), and Plasma cells. **c** Stacked bar plot showing the relative abundance of PBMC subsets across nine samples. Each bar represents the proportion of identified cell clusters. **d** UMAP visualization illustrating the cluster abundance in PBMCs across three groups. The platelet cluster (encircled) is prominently enlarged in the MG group. **e** Boxplot analysis of platelet percentage by group, with statistical significance assessed via one-way ANOVA (two-sided, $p = 0.12$). The boxplot shows the minimum, first quartile, median, third quartile, and maximum values. Dashed lines indicate the comparative percentage of platelets in the same patient pre- and post-treatment. **f** A heatmap showcases the expression of genes related to platelet degranulation across the sample set. **g** Across a larger MG patient cohort, peripheral blood tests confirmed that nGMG patients ($n = 65$) exhibited higher platelet counts compared to HC ($n = 25$, $p = 0.007$) and MMS patients ($n = 40$, $p = 0.0001$). No significant differences were found between nOMG patients ($n = 25$) and the other groups. Data are presented as mean ± s.d., with individual biological replicates shown. *P* values were determined using ordinary one-way ANOVA followed by Tukey's multiple comparisons test. Significance levels are denoted by asterisks: $^{**}p < 0.01$; $^{****}p < 0.0001$. Non-significant results are not depicted. **h** The Circos plot presents the predicted cell-cell communication network, specifically mapping platelet-derived signaling to various immune cell populations in the MG (left, red), HC (middle, blue), and MMS (right, orange) groups. **i**, **j** Bubble plot visualization of platelet-mediated ligand-receptor interactions in MG. Each bubble represents an interaction between platelets and a specific immune cell type, with bubble color indicating the communication probability. The statistical inference method calculates communication probability by comparing the observed ligand-receptor expression against a null distribution generated through cell-label permutation, and assigns *p* values accordingly. **i** depicts incoming signals received by platelets, while **j** represents outgoing signals from platelets to other immune cells. The *y*-axis lists specific ligand-receptor pairs involved in these interactions, providing insight into platelet-driven immune modulation. PBMCs peripheral blood mononuclear cells, HC healthy controls, MMS minimal clinical status, nGMG immunotherapy-naïve generalized myasthenia gravis, nOMG immunotherapy-naïve ocular myasthenia gravis, IST immunological suppressive treatment, UMAP Uniform Manifold Approximation and Projection, Commun. Prob communication probability. Source data are provided as a Source data file.

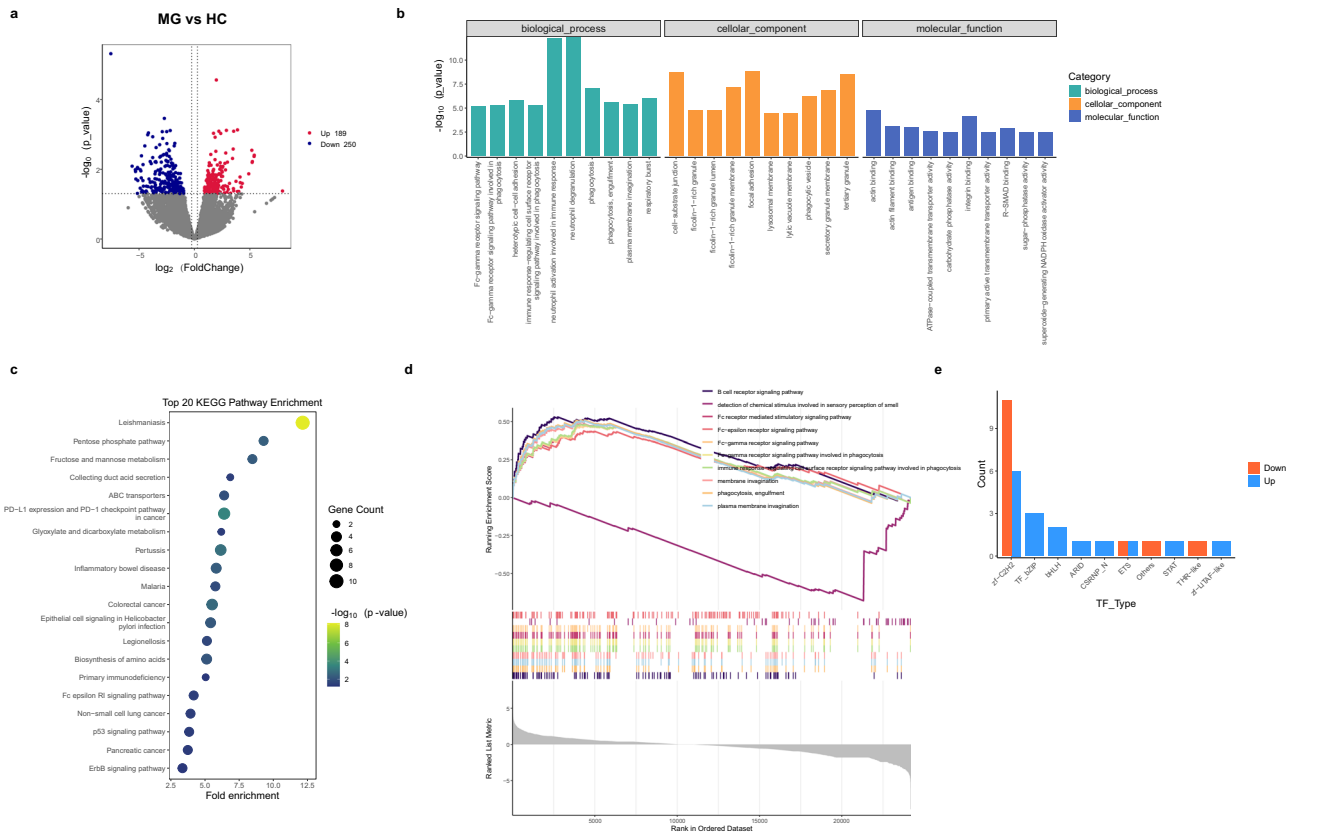

Fig. 3 | Differential gene expression and pathway enrichment analysis in washed platelets from nMG patients and healthy controls using bulk RNA sequencing. a Volcano plot depicting DEGs in platelets between nMG and HC. Upregulated genes ($p \le 0.05$, FC ≥ 1.2) are marked in red, downregulated genes ($p \le 0.05$, FC ≤ −1.2) are marked in blue, and gray dots represent genes with no significant change. Genes selected for clustering analysis met the following criteria: $1 < \max\{\log_2(\text{FPKM} + 1)\} < 20$. Statistical significance was assessed using a two-sided *t*-test, and no adjustments were made for multiple comparisons. **b** GO enrichment analysis of the upregulated DEGs, with significant terms categorized under biological processes, cellular components, and molecular functions. Statistical significance for the enrichment was determined using Fisher's Exact Test (two-sided) for each GO term, with *p* values adjusted for multiple comparisons using Benjamini-Hochberg correction. **c** KEGG pathway enrichment analysis of the top 20 pathways associated with the upregulated DEGs. Pathway enrichment was assessed using Fisher's Exact Test (two-sided), with *p* values adjusted for multiple comparisons using Benjamini-Hochberg correction. **d** GSEA showing enriched pathways in platelets from nMG patients, with color-coded curves indicating significance (red: high enrichment, purple: low enrichment). **e** Classification of TFs based on comparison with the HumanTFDB databases. FC fold change, GO Gene Ontology, KEGG Kyoto Encyclopedia of Genes and Genomes, FPKM fragments per kilobase of exon model per million mapped fragments, TF transcription factor, DEGs differentially expressed genes, nMG immunotherapy-naïve MG, HC healthy controls, MMS minimal clinical status.

https://doi.org/10.1038/s41467-025-63750-2

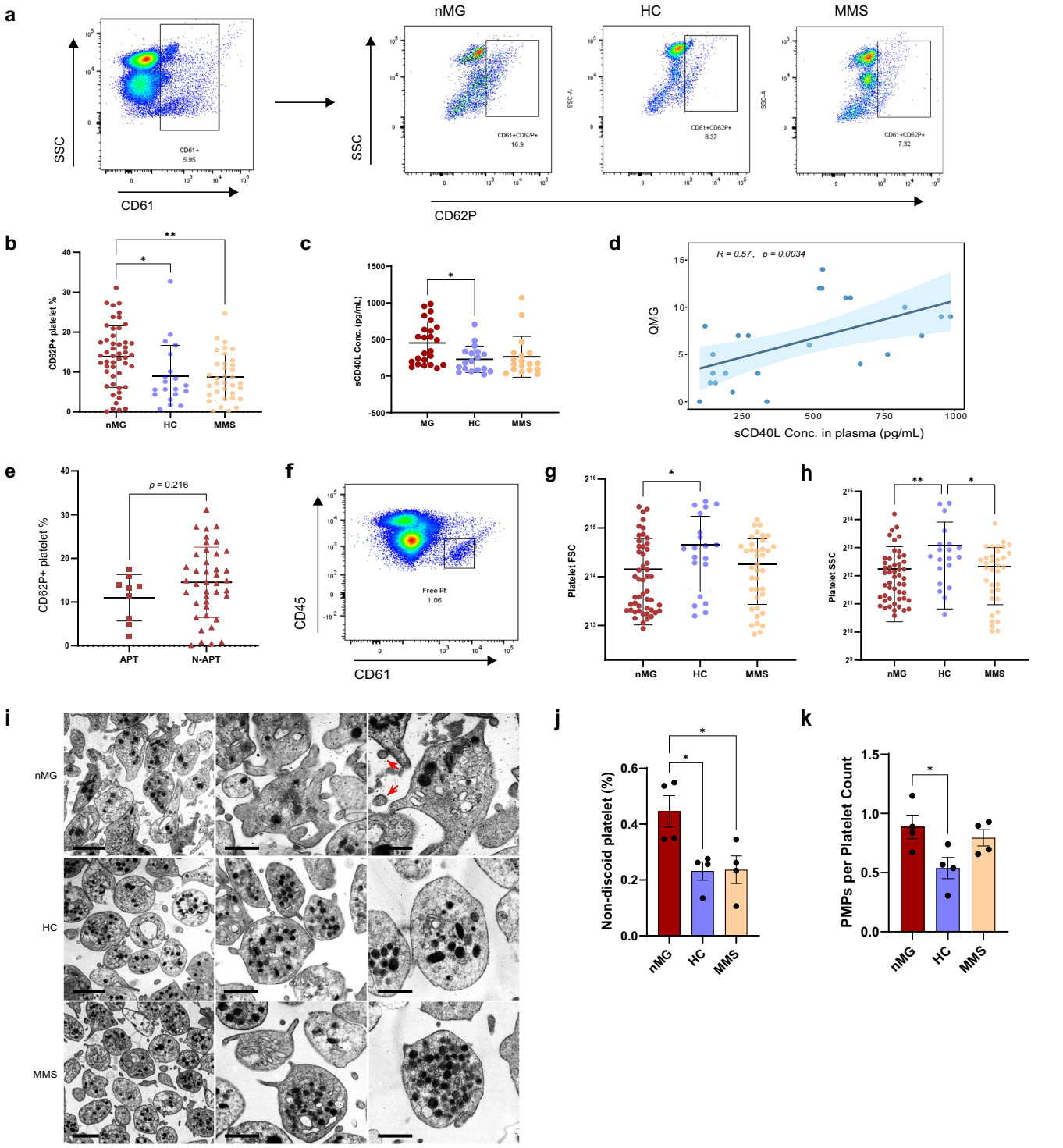

angles of laser light hitting the cells generate forward scatter (FSC) and side scatter (SSC). FSC reflects cell size, while SSC reflects the internal structural complexity or granularity of the cells. Therefore, we further assess the size and morphological changes of nMG platelets by evaluating the FSC and SSC levels of free platelets. The gating strategy for free platelets in peripheral blood flow cytometry is shown in Fig. 4f, followed by analysis of FSC and SSC values for this population using FlowJo software. The results show that nMG patients exhibit a significant reduction in FSC ($p = 0.0124$) and SSC ($p = 0.0032$) values compared to the healthy group (Fig. 4g, h), indicating reduced cellular size and complexity following the release of granular contents during platelet activation. The SSC level in MMS patients is also significantly lower than in the HC group (Fig. 4h; $p = 0.0109$). There are no differences in FSC/SSC between different genders (Supplementary Fig. 3d, e) or APT subgroups (Supplementary Fig. 3f, g). The decrease in the FSC and SSC observed in nMG platelets using flow cytometry is not mirrored in the mean platelet volume (MPV) and platelet distribution width (PDW) parameters obtained from routine blood tests (Supplementary Fig. 2c, d). This divergence could be attributed to the fact that MPV and PDW reflect the average volume and distribution width of the platelet population as a whole, whereas FSC and SSC provide insights into the size and internal complexity of individual platelets. The more detailed single-cell level information provided by FSC and SSC could explain their sensitivity in detecting subtle alterations not apparent in

Fig. 4 | Activation and functional characterization of platelets in nMG patients. **a** Gating strategy for activated platelets and representative flow cytometry scatter plots of CD62P+ platelet populations in nMG, HC, and MMS participants. The left panel shows the initial gating of CD61+ events, followed by further analysis of CD62P expression (right panels). **b** The percentage of CD61+CD62P+ platelets is higher in the nMG ($n = 50$) group compared to HC ($n = 20$, $p = 0.0307$) and MMS ($n = 35$, $p = 0.0037$) groups. **c** A significant increase of sCD40L levels was observed in the nMG ($n = 24$) group compared to the HC group ($n = 18$, $p = 0.0264$). No significant difference was found between nMG and MMS ($n = 18$). **d** Positive association were observed between plasma sCD40L levels and QMG score ($n = 24$, $R = 0.57$, $p = 0.0034$). **e** Influence of APT on the frequency of CD62P+ platelet in nMG patients, with no significant difference observed ($n = 9$ for APT and $n = 41$ for N-APT; $p = 0.216$). **f** Representative flow cytometry scatter plot illustrating the gating strategy for free platelets. The $CD45^{-}CD61^{+}$ population was identified as free platelets, and the FSC/SSC parameters for this specific population were automatically calculated using FlowJo software. **g**, **h** Comparative analysis of FSC and SSC profiles of platelets from nMG ($n = 50$), HC ($n = 20$), and MMS ($n = 35$) participants, showing significant differences in platelet size and internal complexity (FSC: nMG vs HC, $p = 0.0124$; SSC: nMG vs HC, $p = 0.0032$, nMG vs MMS, $p = 0.0109$). **i** Representative transmission electron microscopy images showing platelet morphology in nMG, HC, and MMS groups. Red arrows indicate platelet microparticles. Scale bars: 2 µm in the left column and 1 µm in the middle and right columns. **j** For each patient, we randomly selected five microscopic fields and counted the number of non-spheroid platelets (platelets exhibiting signs of activation, such as filopodia or lamellipodia, deviating from the typical discoid shape) and total platelets within each field. The percentage of non-spheroid platelets was determined by calculating the ratio of non-spheroid platelets to total platelets for each field, followed by averaging the ratios across the five fields. The percentage of non-spheroid platelets was increased in nMG patients ($n = 4$) compared to both HC ($n = 4$, $p = 0.0266$) and MMS ($n = 4$, $p = 0.0295$) groups. **k** The PMP count per platelet was obtained by calculating the PMPs/total platelet ratio for each field and averaging these values across the five fields. The PMPs per platelet count were also increased in the nMG group ($n = 4$) compared with HC ($n = 4$, $p = 0.0466$). For (**b**, **c**, **e**, **g**, **h**, **j**, **k**), data are presented as mean ± s.d., with individual biological replicates shown. Statistical significance was assessed using ordinary one-way ANOVA (two-sided), followed by Tukey's multiple comparisons test, except for (**e**), where an unpaired two-tailed Student's *t*-test was used. For correlation analysis in (**d**), two-sided Spearman's rank correlation was applied, and the regression line is shown with a shaded area indicating the 95% confidence interval. Significance levels are denoted by asterisks: $^{*}p < 0.05$; $^{**}p < 0.01$. Non-significant results are not depicted. nMG immunotherapy-naïve MG, HC healthy controls, MMS minimal clinical status, ADL activity of daily living, QMG score quantitative myasthenia gravis scores, FSC forward scatter, SSC side scatter, APT antiplatelet therapy, Conc. concentration, PMPs platelet-derived microparticles. Source data are provided as a Source data file.

MPV and PDW measurements. Additionally, the higher sensitivity and resolution of flow cytometry enable the detection of minute differences in cell size and internal structure, which might be overlooked in standard blood tests.

To visually demonstrate the platelets' morphological changes in nMG, we conducted transmission electron microscopy (TEM) on washed and purified platelets from four nMG patients, four MMS patients, and four age- and sex-matched HC. Demographic information is provided in Supplementary Table 7. Compared to platelets from HC and MMS, nMG-derived platelets display pronounced morphological deformation, including extended pseudopodia, as shown in Fig. 4i. Quantitative analysis reveals that, on average, nearly half of the nMG-derived platelets (44.6 ± 11.3%) exhibit various morphological signs of activation, such as multiple filopodia or lamellipodia, deviating from the typical discoid shape. In contrast, the proportion of non-quiescent platelets in the HC and MMS groups is 23.2 ± 6.5% and 23.7 ± 9.9%, respectively (Fig. 4j; MG vs HC, $p = 0.0266$, MG vs MMS, $p = 0.0295$). Furthermore, compared to platelets from HC groups, platelets derived from nMG patients display increased presence of PMPs per platelet count (Fig. 4k; $p = 0.0466$), indicating increased degranulation activity.

Collectively, these data substantiate the assertion that platelets exhibit heightened activation in untreated MG, as evidenced by altered characteristics.

Consequences of activated platelets and aggregation with leukocyte formation

To elucidate the interactions between activated platelets and leukocytes, we utilize peripheral blood flow cytometry to simultaneously stain total and subtypes of leukocyte and platelet surface markers. This allows us to compare the proportions of platelet-leukocyte aggregates (PLAs) in the peripheral blood of HC, nMG, and MMS patients. Clinical information for the samples included is provided in Supplementary Table 6. The gating strategy is illustrated in Fig. 5a. Activated platelets in nMG patients exhibit enhanced interactions with leukocytes, forming a greater number of PLAs (Fig. 5b) compared to HC ($p = 0.0034$) and MMS ($p = 0.0002$). No apparent correlation is observed between PLAs and disease severity as quantified by QMG score (Supplementary Fig. 4a; $R = 0.26$, $p = 0.15$). To further explore the nature of these aggregates, we examine different types of PLAs, including platelet-neutrophil aggregates (PNAs), platelet-monocyte aggregates (PMAs), and platelet-lymphocyte aggregates (PLyAs) among the three groups (Fig. 5c–e). A significant increase in circulating PNAs is observed among nMG patients compared to healthy donors ($p = 0.0002$) (Fig. 5c, right), correlating directly with the intensity of disease manifestation ($R = 0.46$, $p = 0.00084$) (Fig. 5f). Following immunotherapy, a discernible decline in these aggregates is observed post-MMS achievement ($p = 0.0002$) (Fig. 5c, right). No significant variations are observed in monocyte- and lymphocyte-platelet aggregates (Fig. 5d, e, right). There are no differences in PLAs/PNAs between different genders (Supplementary Fig. 4b, c) and APT subgroups (Supplementary Fig. 4d, e). Additionally, no significant correlations are found between the proportions of PLAs, PNAs, and the percentage of CD62P+ platelets (Supplementary Fig. 4f, g). The gating strategy for PNAs, PLyAs, and PMAs is shown in Supplementary Fig. 5a–c.

To explore PLA formation in MG following short-term immunotherapy, we assess PLAs frequency before and after intravenous immunoglobulin (IVIg) treatment for 5 days. IVIg has a beneficial therapeutic effect in MG exacerbations through multiple mechanisms[26]. A comparative examination of six exacerbated MG patients (clinical information is detailed in Supplementary Table 8) with moderate to severe symptoms (QMG score 9–24) before and after IVIg treatment discloses a marked decrease in the percentage of PNAs ($p = 0.0032$; Fig. 5g), preceding clinical improvement as assessed by QMG score (before: 15.67 [10.01, 21.33], after: 15.5 [9.72, 21.28]). This highlights the sensitivity of PNAs as an indicator of pathological state shifts over conventional clinical metrics.

Collectively, our results indicate that PNAs correlate with disease severity and decrease post-treatment in MG, suggesting a potential role of platelet-neutrophil interaction in promoting inflammation.

Bidirectional activation between platelets and neutrophils

Previous studies indicate that platelets can induce neutrophil activation and the production of neutrophil extracellular traps (NET)[6], and in turn, NETs can further promote platelet activation[27]. To explore this reciprocal interaction, we co-culture platelets with neutrophils or neutrophil-derived NETs induced in vitro (experimental design is illustrated in Fig. 5h, top panel). Clinical details of the samples included are provided in Supplementary Table 9. Our findings reveal that platelets co-cultured with neutrophils from nMG patients ($n = 7$) exhibit significantly higher activation levels compared to platelets co-cultured with neutrophils from either MMS ($n = 7$) or HC ($n = 7$) groups (Fig. 5i; Plt+nMG_Neu vs Plt+HC_Neu, $p = 0.0002$; Plt+nMG_Neu vs Plt +MMS_Neu, $p < 0.0001$). Additionally, platelets co-cultured with nMG neutrophil-derived NETs ($n = 7$) show enhanced activation compared to those co-cultured with neutrophils from MMS or HC groups (Fig. 5i;

https://doi.org/10.1038/s41467-025-63750-2

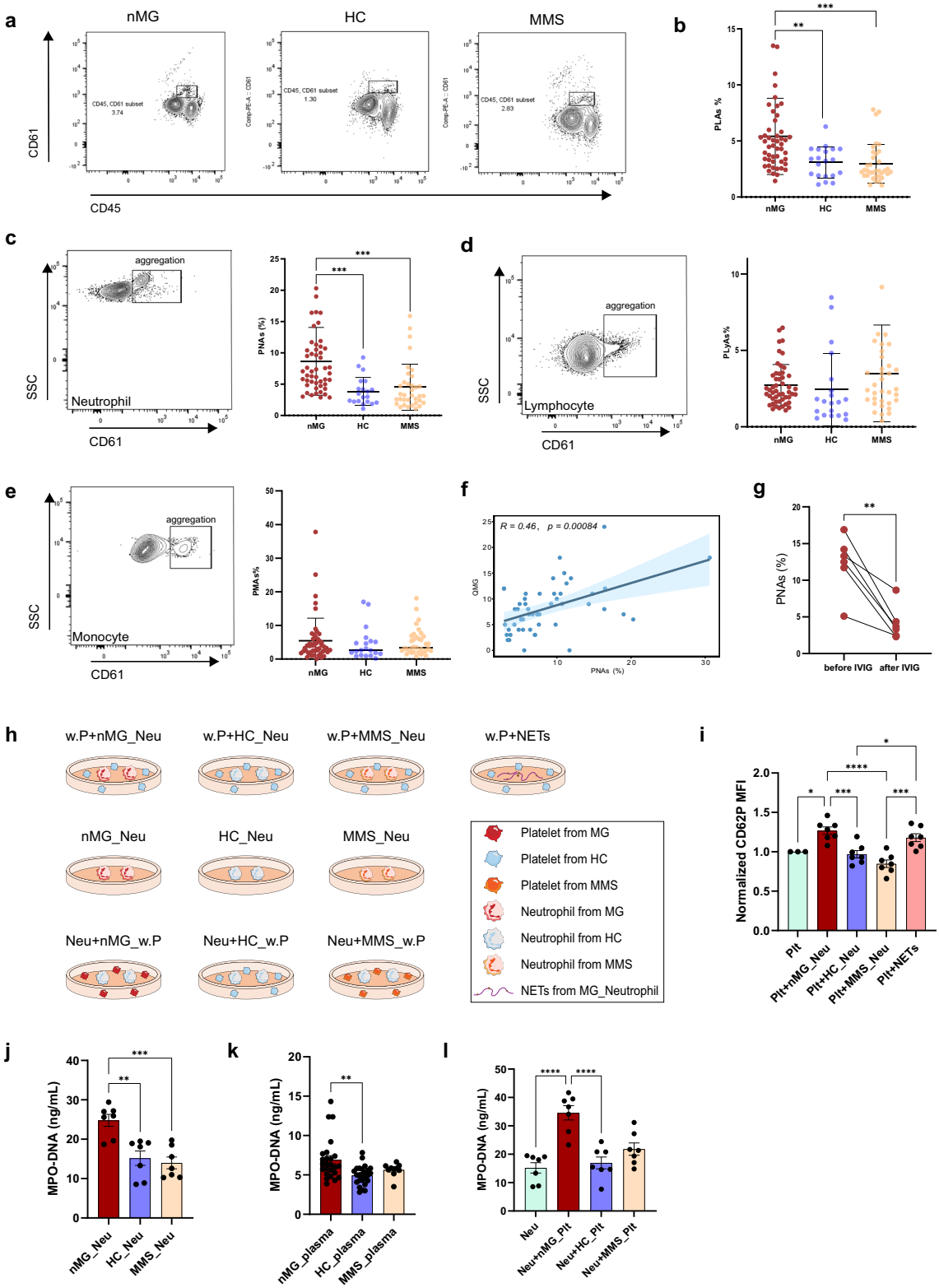

Plt+NETs vs Plt+HC_Neu, $p = 0.0111$; Plt+NETs vs Plt+MMS_Neu, $p < 0.0001$). However, no significant difference in platelet activation is observed when platelets are co-cultured with neutrophils or NETs from nMG patients.

We further examine MPO-DNA levels following overnight culture of neutrophils from different sources (experimental design is illustrated in Fig. 5h, middle panel). Neutrophils isolated from nMG patients form significantly higher levels of NETs compared to those from HC and MMS groups (Fig. 5j; nMG_Neu vs HC_Neu, $p = 0.0016$; nMG_Neu vs MMS_Neu, $p = 0.0005$). Upon expanding the sample size (clinical information is provided in Supplementary Table 10), we also measure MPO-DNA levels in plasma samples from different groups, confirming that plasma from MG patients ($n = 25$) contains significantly higher levels of NETs compared to HC plasma ($n = 25$) (Fig. 5k; MG_Neu

Fig. 5 | Platelet-leukocyte interaction increased in MG. a A representative flow cytometry scatter plot delineates the identification of PLAs within the CD61+ CD45+ population. **b** The dot plot comparison of the percentage of PLAs reveals a statistically significant increase in PLAs among MG patients ($n = 50$) compared to the HC ($n = 20$, $p = 0.0034$) and MMS group ($n = 35$, $p = 0.0002$). **c** A pronounced upsurge in circulating PNAs is observed in MG patients ($n = 50$) compared to HC ($n = 20$, $p = 0.0002$) and MMS group ($n = 35$, $p = 0.0002$), with no significant changes detected in the aggregates involving monocytes and lymphocytes with platelets (**d**, **e**). **f** Positive correlation was observed between the percentage of PNAs and QMG score ($n = 50$, $R = 0.46$, $p = 0.00084$). **g** Significant reduction in PNAs in MG patients following treatment with long-term IST or short-term IVIg therapy ($n = 6$, $p = 0.0032$). **h** Schematic representation of experimental platelet-neutrophil co-culture design. Top row: Platelets were co-cultured with neutrophils from nMG, HC, or MMS patients, or with neutrophil-derived NETs from nMG patients to assess platelets activation. Middle row: Neutrophils from nMG, HC, or MMS patients were cultured overnight to assess NETs formation. Bottom row: Neutrophils were co-cultured with platelets from nMG, HC, or MMS patients to assess NETs formation. **i** Quantification of platelet activation levels (normalized CD62P MFI) after co-culture with neutrophils or NETs from nMG, HC, or MMS patients ($n = 7$ per group). Platelets co-cultured with nMG-derived neutrophils or NETs displayed significantly higher activation levels than those co-cultured with neutrophils from HC or MMS groups ($n = 7$ per group; Plt+nMG_Neu vs. Plt+HC_Neu, $p = 0.0009$, Plt+nMG_Neu vs. Plt+MMS_Neu, $p < 0.0001$, Plt+HC_Neu vs. Plt+NETs, $p = 0.0258$, Plt+MMS_Neu vs. Plt+NETs, $p = 0.0002$). **j** MPO-DNA complex levels in the supernatant following overnight culture of neutrophils from nMG, HC, and MMS patients ($n = 7$ per group). Neutrophils from nMG patients released significantly higher levels of NETs compared to HC or MMS groups (nMG vs. HC, $p = 0.0016$; nMG vs. MMS, $p = 0.0005$). **k** MPO-DNA complex levels in plasma samples from MG ($n = 25$), HC ($n = 25$), and MMS patients ($n = 10$). Plasma from MG patients contained significantly elevated NETs levels compared to HC plasma ($p = 0.0016$). **l** MPO-DNA complex levels in the supernatant following neutrophil co-culture with platelets from nMG, HC, and MMS groups ($n = 7$ per group). Platelets from nMG patients significantly promoted NETs release from neutrophils compared to platelets from the HC group ($p < 0.0001$). For (**b**–**e**, **g**, **i**, **j**–**l**), data are presented as mean ± s.d. with individual biological replicates. For correlation analysis in (**f**), two-sided Spearman's rank correlation was used, and regression lines are shown with shaded 95% confidence intervals. Statistical significance was assessed by ordinary one-way ANOVA with Tukey's multiple comparisons test (**b**–**e**, **i**, **j**–**l**) or paired two-tailed Student's *t*-test. Significance levels are denoted by asterisks: $^{*}p < 0.05$; $^{**}p < 0.01$; $^{***}p < 0.001$; $^{****}p < 0.0001$. Non-significant results are not depicted. nMG immunotherapy-naïve MG, HC healthy controls, MMS minimal clinical status, PLAs platelet-leukocyte aggregates, PNAs platelet-neutrophil aggregates, PLyAs platelet-lymphocyte aggregates, PMAs platelet-monocyte aggregates, QMG score quantitative myasthenia gravis scores, IST immunosuppressive therapy, IVIg intravenous immunoglobulin, NETs neutrophil extracellular traps, MFI mean fluorescence intensity. Source data are provided as a Source data file.

vs HC_Neu, $p = 0.0016$). Collectively, these results suggest that neutrophils from MG patients may contribute to platelet activation via NETs formation.

Additionally, we assess the levels of MPO-DNA complexes in the culture supernatant following co-culture of neutrophils with platelets from nMG, MMS, and HC groups (experimental design is illustrated in Fig. 5h, bottom panel). Clinical details of the samples included are provided in Supplementary Table 9. The results indicate that platelets from nMG patients ($n = 7$) significantly promote the release of more NETs from neutrophils compared to platelets from HC patients ($n = 7$) (Fig. 5i; Neu+nMG_Plt vs Neu+HC_Plt, $p = 0.0009$). These findings align with the observations of increased platelet activation in nMG patients. Taken together, these results suggest that activated platelets play a crucial role in further promoting neutrophil activation and NETs release, establishing a bidirectional interaction between nMG-derived platelets and neutrophils. Specifically, neutrophils from nMG patients activate platelets via NETs formation, while activated platelets further enhance neutrophil activation. This bidirectional activation may contribute significantly to the perpetuation and amplification of systemic inflammation in MG.

Moreover, we observe a trend toward suppression of platelet activation by neutrophils in the MMS group compared to HC (Fig. 5i). However, platelets from the MMS group do not exhibit a similar trend in suppressing neutrophil-mediated NETs formation (Fig. 5l), suggesting that neutrophils may exert a more pronounced influence on platelet activation and phenotype than platelets have on neutrophil behavior.

Platelets from MG patients promote Th1 and inhibit Treg cell responses of human naïve CD4+ T cells in vitro

To elucidate the role of platelets in modulating the adaptive immune response in MG, we investigate the interactions between platelets and Tn cells through in vitro co-culture experiments. For precise assessment and comparison across various samples, the proliferation and differentiation rates of CD4+ T cells are normalized against the levels observed in activated naïve CD4+ T cells (act.Tn) cultured without platelets within the same experimental set. The cut-off value for determining proliferation using CFSE is established using Tn cells not stimulated by CD3/CD28 beads as a control.

Upon activation, platelets modulate CD4+ T cell function through both direct contact and the release of soluble factors[14,28,29]. In our in vitro assays, Tn cells activated with anti-CD3/CD28 beads exhibit substantial aggregation and a proliferation rate of 69.8% ± 20.8% over 3 days, yet without significant differentiation (Supplementary Fig. 6). The introduction of platelets or their supernatants not only intensified T cell proliferation but also modulates Th cell differentiation, underscoring the intricate role platelets play in Tn cell responses within MG.

Furthermore, we compare the proliferation and differentiation of CD4+ T cells after 3 days of direct co-culture with platelets versus indirect co-culture (experimental setup is illustrated in Supplementary Fig. 7), with stimulation using PMA (50 ng/mL) and ionomycin (1 μg/mL) in the presence of BD GolgiStop™ protein transport inhibitor prior to harvesting CD4+ T cells. The gating strategy for proliferated and TNFα/INFγ/IL17A/+Foxp3 CD4+ T cells is shown in Supplementary Fig. 5d–h. We observe that the supernatant from the platelet cultures exhibits a more pronounced effect in enhancing the proliferation of CD4+ T cells compared to direct co-culture with platelets ($p = 0.0490$) (Fig. 6a). In terms of cell differentiation, the platelet supernatant significantly promotes the differentiation of CD4+ T cells into Th1 (IFNγ, $p = 0.0388$; TNFα, $p = 0.0087$) (Fig. 6b, c) and Th17 (IL17A, $p = 0.0068$) (Fig. 6d) subgroups. However, no significant difference is observed in the promotion of Treg (Foxp3) differentiation under both co-culture conditions (Fig. 6e). These findings suggest that the regulatory influence of platelets on the proliferation and differentiation of CD4+ T cells is primarily mediated through a non-direct contact mechanism, reliant on cytokine-mediated pathways. Additionally, the potential impact of contact inhibition effects due to interactions among cell surface molecules should also be considered[14]. In subsequent investigations, we also compare the proliferation of T cells following a 3-day co-culture with platelets in a non-contact setting at various ratios (experimental setup is illustrated in Supplementary Fig. 8), as observed through CFSE staining. Flow cytometry results indicate that the ratio of 1:100 (T cells to platelets) notably enhances T cell proliferation (Fig. 6f).

Based on these findings, we select the 1:100 cell ratio for subsequent experiments. Employing a non-contact co-culture method, we utilize platelet supernatants to explore the effects of platelets from different sources on the proliferation and differentiation of CD4+ T cells. We compare the impact of overnight-cultured platelet supernatants, derived from MG, HC, and MMS patients, on the Tn cell culture system (experimental setup is illustrated in Fig. 6g). Clinical characteristics of platelets and CD4+ T cells co-culture samples are shown in Supplementary Table 11. Microscopy analysis and quantification of cellular aggregate diameters using ImageJ reveal that Tn cells

https://doi.org/10.1038/s41467-025-63750-2

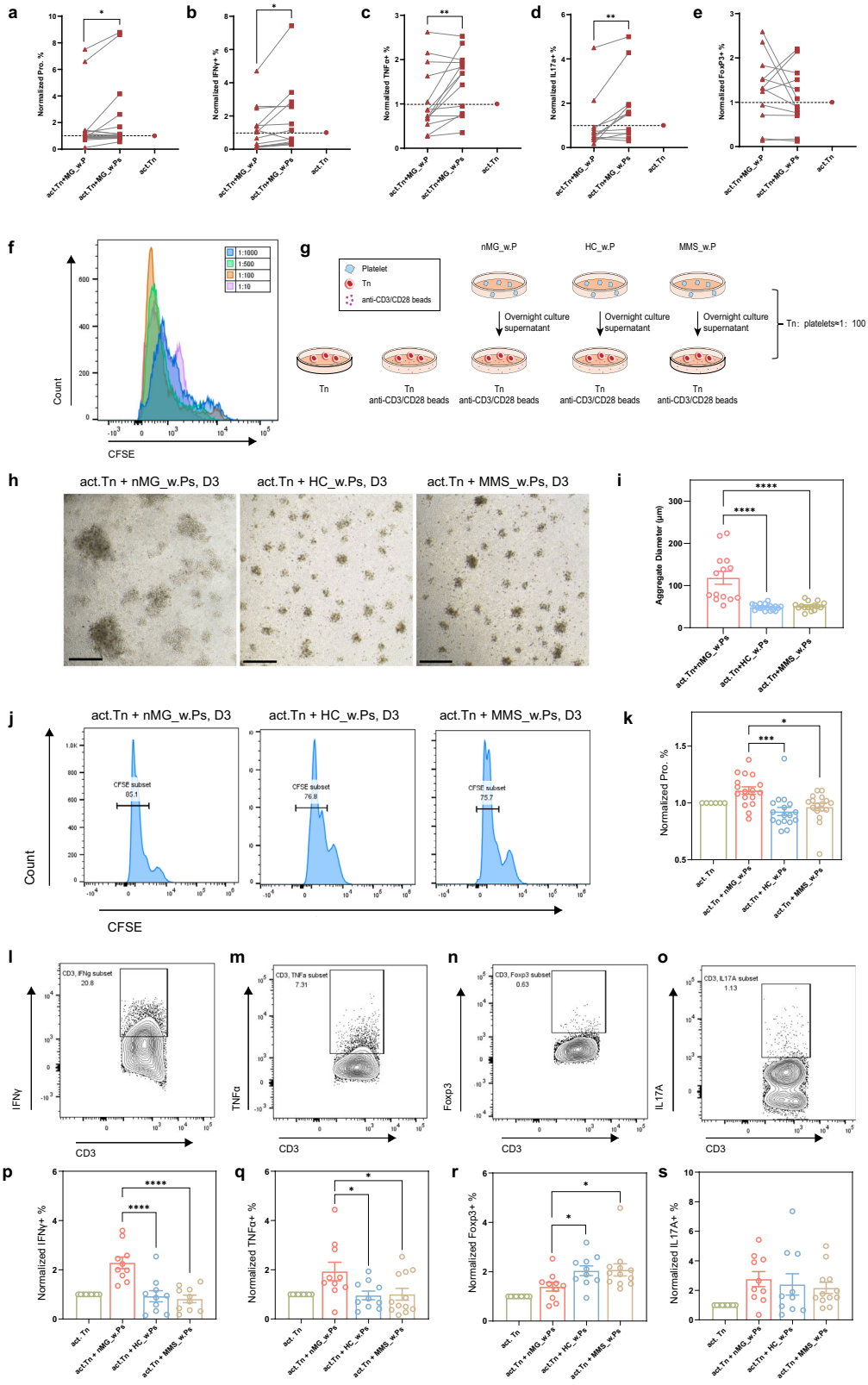

co-cultured with platelet supernatant from nMG patients formed significantly larger aggregates compared to those cultured with platelet supernatant from HC and MMS patients (Fig. 6h, i). This observation is supported by flow cytometry analysis of CFSE Fluorescence attenuation, which shows a marked difference in cell proliferation between the groups (Fig. 6j). Statistical analysis reveals a significant increase in the proliferation of CD4+ T cells in the presence of nMG platelet supernatant, with statistical differences observed when compared to the HC ($p = 0.0008$) and MMS ($p = 0.0105$) groups (Fig. 6k). Further, we assess the differentiation into various subpopulations by evaluating the expression of IFNγ, TNFα, IL17A, and Foxp3 in CD4+ T cells through flow cytometry. The gating strategy is shown in Fig. 6l–o. The data indicate that the proportion of IFNγ/TNFα+ T cells is significantly higher in the group co-cultured with MG platelet supernatant

Fig. 6 | Platelet influence on T Cell proliferation and differentiation. To compare the proliferation and differentiation of CD4+ T cells, stimulation with PMA (50 ng/mL) and ionomycin (1 μg/mL) in the presence of BD GolgiStop™ protein transport inhibitor was performed for 6 h prior to harvesting CD4+ T cells on the fourth day of co-culture. Platelet supernatants, compared to direct co-culture ($n = 18$ per group), significantly amplified the proliferation (**a**) and effector differentiation (**b**–**e**) of Tn cells. A notable increase in the frequencies of proliferated (**a**, $p = 0.049$), IFNγ+ (**b**, $p = 0.0388$), TNFα+ (**c**, $p = 0.0087$), and IL17A+ (**d**, $p = 0.0068$) CD4+ T cells was observed, indicating enhanced inflammatory potential. No significant differences were observed in the frequencies of Foxp3+ CD4+ T cells (**e**). The dashed line represents a baseline value normalized to act.Tn data (normalized to 1). **f** In a separation-based co-culture assay, a platelet-to-Tn cell ratio of 1:100 significantly potentiated the proliferative response of Tn cells, as demonstrated by the dilution of CFSE intensity. **g** We selected the 1:100 cell ratio and employed a non-contact co-culture method for subsequent experiments to compare the impact of overnight-cultured platelet supernatants, derived from MG, HC, and MMS patients, on the proliferation and differentiation of Tn cells. Experimental groups include Tn cells without anti-CD3/CD28 magnetic bead activation; Tn cells cultured alone following activation with anti-CD3/CD28 beads; and activated Tn cells co-cultured with supernatants from washed platelets derived from MG, HC, and MMS patients, at a cell-to-supernatant ratio of 1:100. **h** Representative Microscopy images show that Tn cells co-cultured with washed platelet supernatants from nMG patients (act.Tn + nMG_w.Ps, D3) formed more and larger cell aggregates compared to those co-cultured with HC (act.Tn + HC_w.Ps, D3) and MMS (act.Tn + MMS_w.Ps, D3) supernatants. Scale bar = 200 μm. The statistical analysis of aggregate diameter, measured using ImageJ, is shown in (**i**; $n = 14$ for nMG group, $n = 18$ for HC group, $n = 16$ for MMS group; nMG vs. HC, $p < 0.0001$; nMG vs. MMS, $p < 0.0001$). **j** Corresponding flow cytometry analysis of CFSE fluorescence decay indicates a significant enhancement in CD4+ T cell proliferation in the presence of nMG platelet supernatants. **k** The CFSE subset percentages are shown for each condition, demonstrating the highest proliferation in the nMG group ($n = 17$ for each group, nMG vs. HC, $p = 0.0008$; nMG vs. MMS, $p = 0.0105$). Flow cytometry gating strategies for identifying IFNγ+ (**l**), TNFα+ (**m**), Foxp3+ (**n**), and IL17A+ (**o**) subsets within the live CD3+ T cell population. Comparative analyses of normalized percentages across groups ($n = 10$ per group) show the relative abundance of IFNγ+ (**p**) (nMG vs. HC, $p < 0.0001$; nMG vs. MMS, $p < 0.0001$), TNFα+ (**q**) (nMG vs. HC, $p = 0.0412$; nMG vs. MMS, $p = 0.0431$), Foxp3+ (**r**) (nMG vs. HC, $p = 0.0045$; nMG vs. MMS, $p = 0.0021$), and IL17A+ (**s**) CD4+ T cells upon co-culture with platelet supernatants from various sources. For (**i**, **k**, **p**–**s**), data are presented as mean ± s.d. with individual biological replicates. Statistical significance was assessed by paired two-tailed Student's *t*-test (**a**–**e**) or ordinary one-way ANOVA with Tukey's multiple comparisons test (**i**, **k**, **p**–**s**). Notions of statistical significance are as follows: $^{*}p < 0.05$; $^{**}p < 0.01$; $^{***}p < 0.001$; $^{****}p < 0.0001$; Non-significant results are not depicted. nMG immunotherapy-naïve MG, HC healthy controls, MMS minimal clinical status, Pro. proliferation, Tn cells naïve CD4+ T cells, act.Tn activated naïve CD4+ T, w.P washed platelets, w.Ps washed platelet supernatant. Source data are provided as a Source data file.

compared to the HC group (IFNγ, $p < 0.0001$; TNFα, $p = 0.0412$) (Fig. 6p, q). In contrast, the expression of Foxp3, associated with Tregs, is significantly suppressed ($p = 0.0045$) (Fig. 6r). In patients who reach MMS following immunotherapy, the pro-inflammatory capacity of platelets is notably reduced, with decreased levels of IFNγ ($p < 0.0001$) and TNFα ($p = 0.0431$) (Fig. 6p, q), while Foxp3 associated with Treg differentiation is elevated in the MG group ($p = 0.0021$) (Fig. 6r). Although the platelet supernatant from MG sources appears to promote the proportion of IL17A+ T cells, no statistically significant differences are observed among the three groups (Fig. 6s).

These findings suggest that platelets may play a pivotal role in the pathophysiology of MG, particularly in their interactions with Th cell subsets. This could potentially enhance Th1 cell responses while concurrently attenuating the differentiation of Treg cells, unveiling the potential significance of platelets in the etiology of MG.

RANTES emerges as a pivotal factor in mediating the impact of MG platelets on Tn cell functionality

To delineate the regulatory roles of platelets mediators in Th1/Treg responses within T cells, neutralizing agents for PF4, RANTES, and TGFβ1 are utilized, selected for their regulatory potential and physiological relevance[14,30–32]. Platelet cultures from MG patients and HC are pre-treated with these neutralizing antibodies. Following overnight incubation, platelet supernatants are introduced into Tn cell culture medium. Over 3 days of cultivation, the proliferation and differentiation of Tn cells are evaluated (experimental setup is illustrated in Fig. 7a). Clinical characteristics of co-culture samples are shown in Supplementary Table 12. The results reveal that RANTES neutralization significantly suppressed Tn cell proliferation in both nMG and HC groups (Fig. 7b Columns 1–2, Fig. 7c). This treatment abrogates the enhanced Th1 responses induced by platelets from nMG, while it does not impact Tn cell factors in co-cultures with HC-derived platelets (Fig. 7b Columns 3–4, Fig. 7d, e). Additionally, RANTES neutralization seems to augment Th17 and Treg responses in Tn cells co-cultured with platelets from both nMG and HC, although these effects are not statistically significant (Fig. 7b Columns 5–6, Fig. 7f, g). In the co-culture of platelet supernatants derived from HC, neutralization of TGFβ1 and PF4 promotes T cell proliferation (Fig. 7c). However, this neutralization does not significantly affect the secretion of Th1 cell cytokines (Fig. 7d, e). In the co-culture of platelet supernatants from nMG sources, PF4 neutralization appears to decrease the IFNγ/TNFα+ cell ratio, although this change does not reach statistical significance (Fig. 7d, e).

Furthermore, cytokine analysis reveals that RANTES levels are notably elevated in nMG patient-derived platelet culture supernatants (Fig. 8a; compared with HC: $p = 0.0476$; compared with MMS: $p = 0.0481$), co-cultures (Fig. 8b; compared with HC: $p = 0.0055$), and plasma (Fig. 8c; compared with MMS: $p = 0.0107$). RANTES levels of plasma ($R = 0.5$, $p = 0.013$) and culture supernatants ($R = 0.63$, $p = 0.0095$) in MG patients correlate positively with the QMG score (Fig. 8d, e). Similarly, compared with the HC group, sCD40L levels in MG patient-derived platelet supernatants (Fig. 8f; $p = 0.0264$), co-cultures (Fig. 8g; $p = 0.0159$), and plasma (Fig. 4c; $p = 0.0199$) are concurrently elevated. Intriguingly, a significant positive correlation is observed between plasma levels of sCD40L and RANTES (Fig. 8h; $R = 0.47$, $p = 0.021$), and RANTES neutralization results in a decrease in sCD40L levels (Fig. 8i; $p = 0.0033$) in CD3/CD28-stimulated platelet-Tn cell co-cultures, indicating that the heightened plasma RANTES levels might be attributed to platelet activation.

These observations suggest that RANTES may represent one of the pivotal factors in the platelet supernatant responsible for modulating the inflammatory phenotype of T cells. Neutralization of these cytokines, particularly RANTES, significantly alters the patterns of T cell proliferation and differentiation induced by MG platelet supernatant.

Discussion

In this study, we investigate the role of platelet activation in the pathogenesis of MG. Our findings demonstrate dysregulated platelets activation in MG patients, which correlates with disease severity and is characterized by abnormal morphology, elevated activation markers, and increased PLA formation. Notably, we identify a bidirectional interaction between platelets and neutrophils, wherein neutrophils from nMG patients induce platelet activation via NETs formation, while activated platelets further enhance neutrophil activation and NETs release, perpetuating a pro-inflammatory loop. Additionally, we show that platelets from MG patients modulate Tn cell function by promoting Tn cell proliferation and enhancing Th1 cytokines (IFNγ and TNFα) production, while simultaneously suppressing Treg differentiation (Foxp3). Importantly, RANTES neutralization effectively mitigates these effects, leading to reduced platelet activation and Th1 cytokine production. Collectively, these findings highlight platelet

https://doi.org/10.1038/s41467-025-63750-2

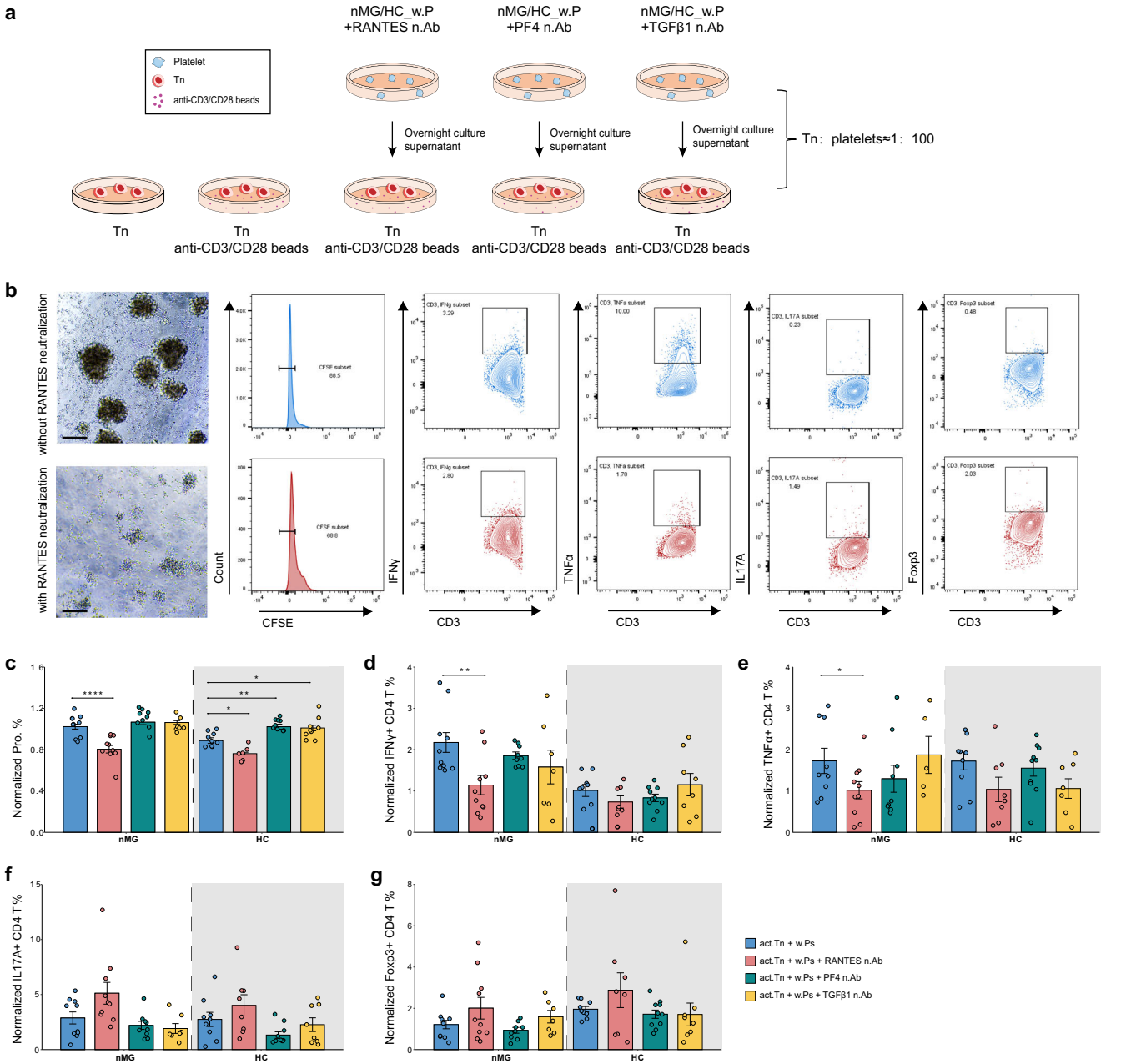

Fig. 7 | Effects of cytokine neutralization on T cell proliferation and differentiation. a Experimental group setup for the platelet cytokine neutralizing antibody experiment. Groups include Tn cells without anti-CD3/CD28 magnetic bead activation; Tn cells cultured alone post-activation with anti-CD3/CD28 beads; activated Tn cells co-cultured with supernatants from washed platelets derived from MG or HC sources, pre-treated with anti-RANTES/PF4/TGFβ1 antibodies, at a cell-to-supernatant ratio of 1:100. **b** Microscopy images reveal less pronounced T cell clustering in conditions where RANTES is neutralized, compared to non-neutralized environments (Column 1). Scale bar: 100 µm. Corresponding flow cytometry profiles demonstrate increased CFSE dilution, indicating suppressed proliferation (Column 2). RANTES neutralization leads to a decrease in IFNγ+ and TNFα+ T cell populations, indicating inhibition of Th1 polarization (Columns 3–4). **c** Quantitative analysis shows that neutralization of TGFβ1 and PF4 in HC-derived platelets enhances Tn cell proliferation ($n = 10$ per group) (IFNγ+ T cell populations: act.Tn+MG_w.Ps vs. act.Tn+MG_w.Ps+RANTES n.Ab, $p < 0.0001$; TNFα+ T cell populations: act.Tn+HC_w.Ps vs. act.Tn+HC_w.Ps+RANTES n.Ab, $p = 0.0278$; act.Tn +HC_w.Ps vs. act.Tn+HC_w.Ps+PF4 n.Ab, $p = 0.0067$; act.Tn+HC_w.Ps vs. act.Tn +HC_w.Ps+ TGFβ1 n.Ab, $p = 0.022$). **d**, **e** The impact of neutralizing antibodies on the frequency of IFNγ+ and TNFα+ T cells is shown ($n = 10$ per group), indicating that neutralization of RANTES suppresses Th1 responses (act.Tn+MG_w.Ps vs. act.Tn +MG_w.Ps+RANTES n.Ab, $p = 0.0064$; act.Tn+MG_w.Ps vs. act.Tn+MG_w.Ps +RANTES n.Ab, $p = 0.038$), while TGFβ1 and PF4 neutralization do not significantly affect Th1 response in either MG patient-derived or control groups. **f**, **g** The frequency of IL17A+ and Foxp3+ Treg cells within Tn cell cultures is depicted, demonstrating the effects of different neutralizing antibodies. For (**c**–**g**), data are presented as mean ± s.d. with individual biological replicates, and statistical significance was assessed by ordinary one-way ANOVA with Tukey's multiple comparisons test. Notions of statistical significance are as follows: $^{*}p < 0.05$; $^{**}p < 0.01$; $^{****}p < 0.0001$. nMG immunotherapy-naïve MG, HC healthy controls, MMS minimal clinical status, Pro. proliferation, Tn naïve CD4+ T, act.Tn activated naïve CD4+ T, w.Ps washed platelet supernatant, n.Ab neutralization antibody. Source data are provided as a Source data file.

https://doi.org/10.1038/s41467-025-63750-2

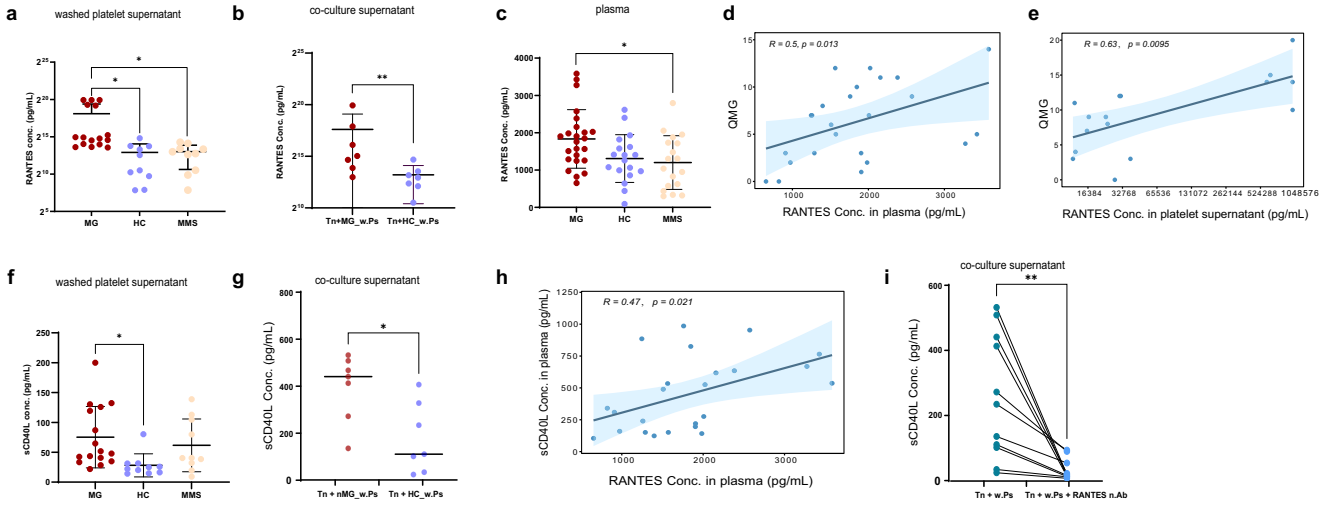

Fig. 8 | RANTES and sCD40L levels in platelet supernatants and co-cultures. **a** RANTES levels were notably elevated in MG ($n = 16$) patient-derived platelet culture supernatants compared to HC and MMS groups ($n = 10$ per group; MG vs MMS $p = 0.0481$; MG vs MMS $p = 0.0476$). **b** Co-culture supernatants show elevated RANTES levels in MG patient-derived platelets co-cultured with Tn compared to HC-derived platelets ($n = 7$ per group, $p = 0.0055$). **c** RANTES levels in plasma were elevated in MG patients ($n = 24$), with a significant increase observed compared to the MMS group ($n = 18$; $p = 0.0187$). No significant differences were detected between MG and HC or between HC and MMS ($n = 18$ for HC). Positive correlations were observed between QMG scores and RANTES concentrations in plasma (**d**, $n = 24$) and platelet supernatants (**e**, $n = 16$). Correlations were assessed using Spearman's rank correlation ($R = 0.5$, $p = 0.013$ for plasma; $R = 0.63$, $p = 0.0095$ for platelet supernatants). **f** sCD40L levels in MG ($n = 16$) patient-derived platelet supernatants were significantly higher compared to the HC group ($n = 10$, $p = 0.0264$). **g** Co-culture supernatants also exhibit increased sCD40L levels in MG patient-derived platelets co-cultured with Tn cells compared to HC-derived platelets ($n = 7$ per group; $p = 0.0159$). A significant positive correlation was observed between plasma levels of sCD40L and RANTES (**h**, $n = 24$), suggesting a potential regulatory relationship. Correlation was assessed using Spearman's rank correlation ($R = 0.47$, $p = 0.021$). **i** RANTES neutralization in CD3/CD28-stimulated platelet-CD4+ T cell co-cultures ($n = 11$) led to a significant reduction in sCD40L levels ($p = 0.0033$), indicating that RANTES influences sCD40L secretion. For (**a**–**c**, **f**, **g**), data are presented as mean ± standard deviation (s.d.) with biologically independent data points shown. For (**i**), data are displayed as individual biological replicates with paired analysis. Statistical comparisons were performed using unpaired two-tailed Student's *t*-tests (**a**, **g**), one-tailed Mann–Whitney *U* test (**b**), ordinary one-way ANOVA followed by Tukey's multiple comparisons test (**c**, **f**), and paired two-tailed Student's *t*-test (**i**). In all correlation plots (**d**, **e**, **h**), regression lines are shown with shaded 95% confidence intervals. Notions of statistical significance are as follows: $^{*}p < 0.05$; $^{**}p < 0.01$. Non-significant results are not depicted. nMG immunotherapy-naïve MG, HC healthy controls, MMS minimal clinical status, QMG score quantitative myasthenia gravis scores, w.Ps washed platelet supernatant, Tn naïve CD4+ T, Conc. concentration, n.Ab neutralization antibody. Source data are provided as a Source data file.

activation as a key contributor to MG-associated inflammation and suggest a potential therapeutic target for modulating immune dysregulation in MG.

Platelets originate from megakaryocytes (MKs) in the bone marrow and, despite lacking a nucleus or DNA, inherit a full transcriptome from their precursor cells. Under physiological conditions, platelet gene expression and splicing remain remarkably stable within individuals over time[33]. However, inflammatory stimuli can trigger the release of platelets with a more complex transcriptomic profile into the circulation. The active spliceosome inherited from megakaryocytes (MKs) dynamically responds to inflammatory cues, invading pathogens, or other stressors, leading to proteomic diversification[34,35]. Our scRNA-seq analysis reveals a significant upregulation of degranulation-related genes in peripheral blood platelets of MG patients compared to HCs and post-treatment conditions. Additionally, bulk RNA-seq highlights a profound shift in platelet function in MG, characterized by heightened immune activation and metabolic reprogramming, indicative of extensive functional remodeling. These findings underscore the critical role of platelets in MG pathophysiology, aligning with previous studies implicating platelet dysfunction in autoimmune disorders[36]. Jin et al.[37] identify significant differences in bone marrow-derived cell populations in MG patients compared to HC using single-cell PBMC analysis. This finding suggests a potential dysregulation of the bone marrow microenvironment, which may contribute to the peripheral expansion of functionally active platelets in MG. Given the emerging recognition of platelets as central mediators of immune regulation and inflammation, it is plausible that these hyperactive platelets further amplify inflammatory cascades in MG, thereby exacerbating disease pathology.

Our study reveals morphological alterations in MG platelets, notably a reduction in cell size and heightened microparticle release, which are aligned with the enhanced degranulation activity detected through transcriptome analysis. Such changes, specifically the decrease in size and granularity reflected by FSC and SSC, are indicative of a platelet activation-dependent mechanism. Activation is characterized by the release of intraplatelet calcium, leading to the actin-myosin cytoskeleton activation. This process results in a transformation from the typical discoid shape to a spherical conformation with lamellipodia extensions[38], a pattern also observed in patients with active SLE and chronic rheumatic disease, where diminished platelet size correlates with microparticle formation and disease activity[39–41]. Additionally, we observe that patients with a higher proportion of CD62P-positive platelets tend to exhibit lower granularity, as indicated by reduced platelet SSC measurements. This supports the notion that smaller platelet size is associated with activation and degranulation processes in autoimmune diseases.

Platelet activation triggers the translocation of CD62P from α-granules to the membrane surface, facilitating aggregate formation through binding to the high-affinity counter-ligand PSGL-1 on leukocytes[33]. Given the high expression of PSGL-1 on neutrophils and their substantial presence in peripheral blood[42,43], PNAs emerge as a key biomarker for disease severity in various autoimmune disorders[41,44–46]. In MG, we observe a significant elevation in PNAs, underscoring their involvement in disease pathology. Notably, immunotherapy targeting MG effectively reduces platelet activation

and consequently decreases PNAs, highlighting their potential as both a disease marker and a therapeutic target. Mechanistically, in vitro studies demonstrate that PNAs mediate platelet-driven modulation of neutrophil chemotactic and cytotoxic functions[25,47]. In both in vitro and immunocompromised mouse models, activated platelets interact with neutrophils to enhance autophagy, characterized by granule mobilization, enhanced proteolytic activity, prolonged cell survival, and NETs formation[45]. Furthermore, platelet membrane molecules such as GPIV, GPIIb/IIIa, and CD40L serve as synergistic stimulators of neutrophil activation, exacerbating inflammation[48]. In contrast, platelet-monocyte and PLyAs exhibit no significant alterations, suggesting that neutrophils, rather than monocytes or lymphocytes, are the predominant mediators of platelet-driven inflammation in MG. This distinction likely stems from the pivotal role of neutrophils in the inflammatory cascade, as they are more readily activated and prone to forming aggregates with platelets, particularly in systemic inflammation[49]. Conversely, platelet interactions with monocytes and lymphocytes may require more specific activation conditions to elicit measurable effects[50]. Importantly, the dynamic interplay between platelets and neutrophils appears highly responsive to the immunomodulatory effects of MMS therapy, further reinforcing the critical role of neutrophils in MG pathogenesis.

Through further investigation into platelet-neutrophil interactions, we identify a bidirectional and mutually reinforcing interplay between these cells in the pathogenesis of MG. Notably, platelets co-cultured with neutrophils from nMG patients exhibit a heightened activation state comparable to that induced by direct exposure to NETs, underscoring the pivotal role of NETs in platelet activation. Moreover, significantly elevated levels of NETs were detected in both the co-culture supernatant and plasma of nMG patients, further substantiating this association. These findings align with previous studies that demonstrate NETs, by exposing pro-inflammatory molecules and promoting platelet aggregation, contribute to an inflammatory milieu[51,52]. Interestingly, compared to platelets from MMS or HC groups, platelets from nMG patients exhibit an enhanced capacity to induce NETs formation in neutrophils. This suggests that platelet activation in MG potentiates neutrophil activation and NETs release, which, in turn, further amplifies platelet activation. Such a positive feedback loop may play a critical role in sustaining and exacerbating systemic inflammation in MG, potentially driving disease progression. Notably, while neutrophils from MMS patients exhibit a degree of suppressive effect on platelet activation, MMS platelets did not reciprocally suppress NET formation in neutrophils. This asymmetry suggests that, within the MG pathophysiological process, the influence of neutrophils on platelets may be more pronounced than the reverse effect. Of course, Platelet activation is a complex process driven by an array of surface receptors that respond to diverse stimuli[6], with neutrophil-mediated activation representing only one such mechanism. In MG, platelet activation appears to be a secondary event following systemic immune-inflammatory responses. However, once activated, platelets may further modulate both innate and adaptive immune cells, thereby intensifying inflammation and perpetuating disease progression.

Beyond the aforementioned cell membrane interactions governed by ligand-receptor dynamics, platelet activation also modulates immune cell functionality via secreted soluble factors[53]. In our study, we observe that platelets from MG patients significantly boost CD4+ T cell proliferation and modulate Th1 and Treg cell responses in vitro. Interestingly, the platelet supernatant proves more potent in promoting Tn cell proliferation and differentiation than direct co-culture, highlighting the significance of these soluble factors. While RANTES neutralization dose not affect Th1 responses in platelet co-cultures derived from healthy individuals, it considerably reduces such responses in the MG patient-derived platelets group, aligning IFNγ/TNFα+ T cell levels with those in Tn cells co-cultured with HC-derived platelets. This variant impact on modulating immune responses depending on the different platelet sources, and the elevated RANTES levels in MG platelet cultures and plasma indicate its potential role in fostering an inflammatory T cell phenotype in MG. Previous studies show that RANTES interaction with the CCR5 receptor on T cells activates crucial pathways like JAK/STAT and AKT/mTOR, vital for T cell responses[54,55]. The heightened expression of RANTES in MG patients' thymus suggests its involvement in thymic inflammation and lymphocyte recruitment[56]. This is supported by the effectiveness of JAK2 inhibitors in experimental autoimmune MG, implicating a role for the JAK/STAT pathway in MG pathogenesis[57]. Given these observations, we speculate that activated platelets in MG might trigger the JAK/mTOR pathway in T cells via the RANTES-CCR5 axis, influencing the TFs associated with T cell-mediated immunity in MG, which merits further exploration.

While the MMS group demonstrates improvements in many measures (e.g., platelet count, formation of PLAs) and does not show statistically significant differences compared to the HC group, it is possible that platelet activation states do not completely revert to the HC phenotype due to residual disease activity or incomplete resolution of inflammation. Additionally, the treatments used in the MMS group may directly or indirectly modulate platelet activation, leading to persistent differences. In fact, we observe other indications suggesting that MMS platelets have not fully returned to the normal phenotype. For example, electron microscopy shows that MMS platelets have a higher level of PMPs number per platelet (Fig. 4k), and the NETs formed by neutrophils co-cultured with MMS platelets remain slightly elevated compared to HC group (Fig. 5h). Furthermore, CD4+ T cell proliferation in the presence of MMS platelet supernatant is higher than in the HC group (Fig. 6k). Taken together, these findings suggest that platelets in the MMS group may remain mildly activated or exhibit a tendency for activation compared to HCs. This tendency may relate to the potential for relapse in MMS patients and warrants further investigation in future studies.

In conclusion, our investigation pioneers the examination of platelet involvement in the mechanism of MG. We elucidate the pivotal and previously unexplored role of activated platelets as central contributors to MG pathogenesis, particularly through the mediation of Th cell inflammatory responses. Our innovative findings reveal that PNAs and cytokines from activated platelets hold promise as innovative biomarker candidates for the development and prognosis of MG. Further inquiries into the precipitators of platelet activation in MG, the impact of platelet-derived molecules on disease progression, and the identification of other critical ligands, in conjunction with RANTES, that drive Th1 differentiation and Treg dysfunction, are anticipated to deepen our understanding of MG pathogenesis. These investigations may enhance our understanding of MG pathophysiology and inform the development of targeted therapeutic approaches.

Methods

Study participants and sample collection

In this study, we enrolled 209 nMG, 119 patients in minimal manifestation status (MMS) following treatment, and 114 age- and sex-matched HCs. The sex of participants was recorded, and participants' sex was determined based on self-report. The participant screening and enrollment process is illustrated in Fig. 1. For nMG and MMS patients, they were recruited from the Department of Neurology at Xuanwu Hospital, between June 2021 to October 2023. All patients were above 35 years old, with an average age of 53–55 years, as presented in the supplementary tables. Patients were excluded based on the following criteria: (1) non-AChR-MG; (2) less than 18 or more than 80 years old; (3) history of malignant tumors (except thymoma) and other autoimmune diseases; (4) pregnancy; (5) incomplete clinical data or abnormal flow cytometry data. The diagnosis of MG was made in accordance with international guidelines[58]. We collected data on sex,

age, disease course, Myasthenia Gravis Foundation of America classification[23], MG subtypes (including GMG, ocular MG[OMG], and thymus status), and laboratory data (including platelet count, neutrophil count, lymphocyte count, MPV, PDW, and serum antibody assay). The QMG score was used to evaluate disease severity at the time of enrollment and the therapeutic effect after immunotherapy treatment. The HCs were selected from the hospital medical staff, nurses, and their family members. All controls underwent thorough medical examinations to rule out any autoimmune diseases, cancer, chronic infections, and other underlying health conditions.

The first cohort was utilized for the 10× genomics scRNA-seq, including three HCs and three GMG who had not yet commenced immunosuppressive therapy. These three patients received corticosteroids and/or immunosuppressant for treatment, with two of them achieving and maintaining MMS. These two patients (nMG1 and nMG3) underwent scRNA-seq again to analyze the overall cell proportional and transcriptional changes related to MG disease activity. The validation cohort was used for bulk RNA sequencing, laboratory data analysis, flow cytometry analysis, morphological examination, and functional assays, comprising age- and sex-matched HCs ($n = 111$), newly diagnosed nMG ($n = 201$), and MG patients who reached MMS or better ($n = 119$). Detailed patient demographics and clinical characteristics are outlined in Supplementary Tables 1 and 3–12.

All uses of human material were approved by the Ethics Committee of Xuanwu Hospital, Capital Medical University (Approval No. 2017084). Participants provided written informed consent to participate in the study before taking part. Healthy volunteers disclosed not taking any medication during the 2 weeks prior to blood sampling.

10X Genomics single-cell sequencing of peripheral blood mononuclear cells

For each participant, 6 mL of venous blood was drawn into tubes containing EDTA as an anticoagulant and promptly transported to the laboratory under refrigerated conditions. PBMCs were then isolated from these samples utilizing density gradient centrifugation via Ficoll-Paque medium (Dakewe, 7111011). This was followed by three successive washes in 0.04% BSA DPBS, ensuring thorough cleansing. Cell viability was ascertained to be in excess of 95% using the Countess® II Automated Cell Counter. For each sample, cell suspensions were calibrated to contain approximately 13,000 cells.

Single-cell RNA sequencing libraries were constructed using Chromium Single Cell 5′ Reagent Kits v3 (10x Genomics), following the manufacturer's guidelines. The libraries, consisting of paired-end reads with a length of 150 bp, were sequenced on the NovaSeq 6000 (Illumina). Raw data of Fastq files underwent initial quality control, with demultiplexing and alignment to the GRCh38 V3.0.0 human reference genome, using the 10x Genomics Cell Ranger pipeline. Unique molecular identifiers (UMIs) were mapped to genes, and barcodes were assigned to cells. Anchor-based integration was used to harmonize single-cell data across multiple experimental conditions. Aggregated data were further analyzed using Seurat (v3.1.2) in R (v3.6.3). Secondary data filtering was performed, retaining genes expressed in a minimum of three cells and cells expressing at least 200 genes. Cells expressing less than 500 or more than 3500 genes, or those with over 7% of UMIs mapped to mitochondrial or ribosomal genes, were excluded.

The expression data was followed by log-normalization and scaling of single-cell transcriptome data to enable a thorough analysis. For dimensionality reduction, we conducted Principal Component Analysis employing the Seurat package, retaining 20 principal components based on the Jackstraw method. For identification of cluster-specific marker genes within transcriptional subpopulations, the FindAllMarkers function in Seurat was utilized, applying the Wilcoxon rank-sum test. A p value threshold of <0.05 post-Benjamini-Hochberg False Discovery Rate correction was set for statistical significance. The identities of the clusters were manually annotated by leveraging known marker genes, as cited in high-quality scRNA-seq publications[37,59], which are listed in Supplementary Table 13. The results were visually rendered using the ggplot2 package (v3.4.2). Beyond profiling cell-intrinsic states, scRNA-seq data were further analyzed to infer cell-extrinsic signaling interactions. For this, we used the CellChat package (v2.1.2) to explore platelet-associated intercellular communication among MG, HC, and MMS groups. Default settings were used to predict ligand-receptor interaction pairs, and results were visualized using circle and bubble plots.

Bulk RNA sequencing of purified, washed platelets

Obtaining purified, washed platelets. Blood was collected in sodium citrate tubes and used within 15 min. Platelets isolation involved processing 6 mL of citrated blood immediately post-collection. The initial centrifugation step (190 g, 20 min, 22 °C) yielded platelet-rich plasma (PRP), from which the upper 2/3 was collected. A fraction of these samples was preserved at −80 °C for subsequent cytokine analysis. The remaining PRP underwent further centrifugation (190 g, 10 min, 22 °C) in the presence of 0.1 μg/mL prostacyclin I_2 (PGI_2) (MedChemExpress, HY-A0126A). The secondary PRP was collected and re-spun (1,000 g, 10 min, 22 °C), and the pellet obtained was resuspended in Tyrode's-HEPES buffer (Procell, PB180340) supplemented with 10 μM indomethacin (MedChemExpress, HY-14397A) and 0.1 μg/ mL PGI_2. Finally, the platelets were pelleted, resuspended in Roswell Park Memorial Institute (RPMI) 1640 (HyClone, SH30027.01) culture medium at a density of 1 ×108 platelets/mL, and maintained at RT for 30 min to allow the restoration of platelet responsiveness.

Bulk RNA seq. For bulk RNA sequencing, purified, washed platelets were isolated from three nMG and three HC individuals. Full-length cDNA and sequencing libraries were prepared using the Illumina Smart-seq2 protocol[60]. The concentration of the amplified cDNA products was measured using the Qubit® 3.0 Fluorometer (Life Technologies, CA, USA). The fragment distribution of the amplified cDNA samples was assessed using the Fragment Analyzer 1.0.2.9. The libraries were then sequenced on the Illumina MiSeq platform to generate 35-base paired-end reads. Hisat2 was used for read alignment, and featureCounts v1.5.0-p3 was employed to quantify the number of reads mapped to each gene. The fragments per kilobase of transcript per million mapped reads (FPKM) for each gene were calculated based on gene length and the read count for each gene.

DEGs were identified using the DESeq2 R package (v1.16.1) with a significance threshold of $p < 0.05$ and a fold change >2 or <−2. GO enrichment analysis and statistical testing of DEGs in KEGG pathways were performed using the clusterProfiler R package (v4.6.1). Additionally, GSEA was implemented with clusterProfiler to identify enriched biological pathways.

Peripheral blood flow cytometry analysis

Peripheral blood flow cytometry analysis was utilized to evaluate the expression of CD62P on platelets and the formation of aggregates. Peripheral blood samples were collected through venipuncture at the antecubital vein using siliconized vacutainers containing 3.8% sodium citrate (1/10 volume) and processed within 15 min. Whole blood samples underwent red blood cell lysis buffer (Solarbio, R1010) to remove erythrocytes. The remaining leukocytes and platelets were washed in phosphate-buffered saline (PBS) (Solarbio, P1020) with 1% BSA (Miltenyi, 130-091-376) and resuspended for further analysis. Briefly, peripheral blood samples were incubated with fluorochrome-conjugated anti-human antibody mix, including FITC-labeled anti-CD62P (1:100 dilution; Biolegend, 304903), BV421-labeled anti-CD15 (1:50 dilution; Biolegend, 323039), PE/Cyanine7-labeled anti-CD14 (1:300 dilution; Biolegend, 325617), PerCP-labeled anti-CD45 (1:100 dilution; Biolegend, 368505), and PE-labeled anti-CD61 (1:100 dilution; Biolegend,

336405), for 30 min in the dark at room temperature (RT). After staining, cells were washed in 1x PBS and acquired at BD FACSAria III (BD Biosciences) using BD FACSDiva™ Software v8.0 (BD Biosciences). Data were analyzed using FlowJo software v10.8.0 (TreeStar).

Morphological examination

TEM was employed to scrutinize the ultrastructural characteristics of platelets directly isolated from whole blood of individuals with MG, HC, and MMS, as described in "Obtaining purified washed platelets." For this analysis, purified platelet cell pellets were collected and fixed with 4% paraformaldehyde (Solarbio, P1110) at 4 °C for a duration of 2 h. Subsequent to fixation, the pellets underwent a series of washes with PBS (Solarbio, P1020) at pH 7.2, three times, each for 10 min. For further fixation, 1% osmium tetroxide was employed at 4 °C for 2 h, followed by triple rinsing with distilled water, with each rinse lasting for 10 min. A graded dehydration process was implemented using ethanol (General Reagent, P3223264) concentrations of 50%, 70%, and 90%, for 10 min at each concentration, followed by dehydration in 100% ethanol twice, each for 15 min. The samples were then subjected to two 15-min exchanges in propylene oxide (HUSHI, 80059118), followed by infiltration with a mixture of propylene oxide and resin in ratios of 1:1 and 1:4 for 1 h each, and finally in pure resin for 2 h. Embedding was carried out using EPON 812 pure resin (SPI, 1280505), with polymerization stages set at 45 °C, 60 °C, and 80 °C, each for a duration of 5 h. Ultrathin sections of 90 nm were prepared and stained with uranyl acetate (SPI-CHEM, 1121018) and lead citrate (Electron Microscopy Sciences, 17800). Finally, cellular morphology was examined using a JEM-1400 electron microscope.

To quantify the percentage of activated platelets and PMPs, blind counting was independently performed by different researchers. The final values were obtained by calculating the average from these double-blind counts.

Platelet-neutrophil ex vivo interaction

Neutrophil isolation. Neutrophils were isolated using the CD66abce MicroBead Kit (Miltenyi, 130-092-393) according to the manufacturer's protocol. Briefly, neutrophils were extracted from lysed whole blood using Blood Cell Lysis Buffer (Solarbio, R1010), followed by positive selection of CD66b-expressing cells with biotinylated anti-human CD66b antibody (1:5 dilution). After incubation and washing, CD66b-positive cells were enriched using anti-Biotin MicroBeads. The isolated neutrophils, with a purity >95% confirmed by flow cytometry, were suspended in RPMI-1640 medium at 1×10^6 cells/mL.

Platelet-neutrophil co-culture. To investigate the potential role of platelet-neutrophil interactions in the pathogenesis of MG, we performed platelet-neutrophil co-culture experiments. Isolated platelets and neutrophils were co-cultured at a ratio of 100:1 in RPMI-1640 culture medium supplemented with 10% fetal bovine serum (FBS; Gibco, 26170043) and 1% penicillin-streptomycin (Beyotime, C0222), under standard conditions (37 °C, 5% CO_2) for 24 h. The supernatants were collected and stored at −80 °C for NETs detection.

In certain experiments, we extended our analysis to include co-cultures of platelets with neutrophil-derived NETs to evaluate the impact of NETs on platelet activation. Neutrophils from nMG patients were cultured overnight at a concentration of 1×10^6 cells/mL. The culture supernatant was collected by centrifugation at $300 \times g$ for 10 min, removing cell debris, resulting in the isolation of NETs. The supernatant containing the NETs was then added to the platelet culture system. This approach allowed for the examination of the role of NETs in modulating platelet activation.

Platelet activation assay. After 24 h of co-culture, cells were harvested for flow cytometric analysis to assess platelet activation. Platelets were identified by the surface marker CD61 (PE-labeled anti-CD61; 1:100 dilution; Biolegend, 336405), and platelet activation was assessed by measuring the mean fluorescence intensity (MFI) of the activation marker CD62P (FITC-labeled anti-CD62P; 1:100 dilution; Biolegend, 304903). The level of CD62P expression, which is a well-established marker of platelet degranulation and activation, was compared across the different experimental groups to determine the extent of platelet activation.

NETs detection. Plasma samples from MG, MMS, and HC patients, as well as platelet-neutrophil co-culture supernatants, were collected for NETs analysis. MPO-DNA complexes, which serve as markers of NET formation, were quantified, with an increase in their levels indicating enhanced NET formation. To capture MPO-DNA complexes, 5 μg/mL of anti-MPO monoclonal antibody (Proteintech, 22225-1-AP) was coated onto a 96-well plate and incubated overnight at 4 °C. After blocking with 1% BSA, 100 μL of diluted serum was added to each well and incubated at room temperature for 2 h on a shaker. Following incubation, the plates were washed five times with PBST (Solarbio, P1033). According to the manufacturer's instructions, PicoGreen dsDNA Quantitation Reagent (Yeasen, 12641ES01) was then added. The fluorescence intensity of the samples was measured using a fluorometer with an excitation wavelength of 480 nm and an emission wavelength of 520 nm. The MPO-DNA complexes in the samples were quantified using DNA standards for semi-quantitative analysis.

Platelet-Tn ex vivo interaction

Naïve CD4 T cell isolation. PBMCs were isolated as outlined in section "10X genomics single-cell sequencing of peripheral blood mononuclear cells." Subsequently, naïve CD4+ T (Tn) cells were purified using MojoSort™ Human CD4 Naïve T Cell Isolation Kit (Biolegend, 480041), following the manufacturer's instructions. The isolated Tn cells, with a purity >95% as verified by flow cytometry, were suspended in RPMI-1640 medium at a concentration of 1×10^6 cells/mL.

Preparation of washed platelets and overnight culture supernatant. To mitigate the potential impact of non-platelet-derived mediators present in platelet-rich plasma or preservatives in platelet concentrates, washed platelets were utilized for the co-culture experiments. Purified washed platelets were placed in a CO_2 incubator set at a constant temperature. The supernatant was collected the following day, with a portion allocated for co-culturing with Tn cells, and the remainder was collected and centrifuged at $3000 \times g$ for 10 min, filtered with 0.22 μm filters (Sigma-Aldrich, USA), and stored at −80 °C for cytokine analysis.

Co-culture experimental setup. Purified Tn cells were obtained and pre-labeled using CFSE (Carboxyfluorescein Succinimidyl Ester) staining as described in the CFSE Cell Division Tracker Kit (5 μM; Biolegend, 423801). The activation of Tn cells was induced using Dynabeads™ Human T-Activator CD3/CD28 for T Cell Expansion and Activation (Gibco, 11161D; at a concentration of 1×10^6/mL). To precisely determine the optimal cell ratio and co-culture conditions between Tn cells and platelets, washed platelets were prepared at varying concentrations according to the Tn cells to platelets ratios tested (1:10, 1:100, 1:500, and 1:1000) in a total volume of 200 μL. After comparing the results of direct co-culture across different ratios, we identified 1:100 as the optimal ratio for Tn cell activation and platelet interaction. Using this ratio, we compared the effects of direct (physical contact) and indirect (supernatant-dependent) co-culture (Supplementary Figs. 7 and 8).

In the formal experiments, a non-contact co-culture approach was adopted. Platelet supernatants collected after overnight incubation were added to the Tn cell culture wells, with control groups

established. The cells were then incubated at 37 °C in 5% CO_2 for 3 days, during which cell aggregation and proliferation were monitored daily under a microscope and documented through photography.

Stimulation and cell staining. On the fourth day of co-culture, the supernatant was collected and centrifuged at 3000 × *g* for 10 min, filtered with 0.22 μm filters, and stored at −80 °C for subsequent cytokine analysis. Fresh culture medium was added to the CD4+ T cells, followed by stimulation with Phorbol 12-myristate 13-acetate (PMA, 50 ng/mL) and ionomycin (1 μg/mL) (Cell Activation Cocktail; Biolegend, 423302) in the presence of BD GolgiStop™ protein transport inhibitor (BioLegend, 420701) for 6 h. After stimulation, cells were transferred to EP tubes and subjected to a magnetic field to attract magnetic beads, then moved to flow cytometry tubes. The cells were washed, stained with Zombie dye (1:500 dilution; BioLegend, 423105) to assess viability, and labeled with PerCP-labeled anti-CD3 (1:100 dilution; BioLegend, 300427). For intracellular cytokine staining, the cells were then treated with Fix/Perm solution (Biolegend, 420801) and re-stained with PE/Cyanine7-labeled anti-IFNγ (1:100 dilution; Biolegend, 502527), PE-labeled TNFα (1:100 dilution; Biolegend, 502908), and Brilliant Violet 421™-labeled IL17A (1:100 dilution; Biolegend, 512321). For TF staining, the cells were treated with True-Nuclear™ Transcription Factor Buffer Set (Biolegend, 424401) after surface staining and re-stained with Alexa Fluor® 647-labeled anti-Foxp3 (1:200 dilution; Biolegend, 320013).

Flow cytometry analysis. Flow cytometry analysis was performed using a BD FACSAria III cytometer (BD Biosciences). Following staining, cells were acquired and analyzed using FlowJo software v10.8.0 (TreeStar). The proliferation and differentiation of T cells were quantified as the percentage of proliferated or differentiated T cells and normalized against anti-CD3/CD28 bead controls. The cytokine production of CD4+ T cells (IFNγ, TNFα, IL17A) was assessed to evaluate inflammatory responses, while Foxp3 expression was used to determine Treg differentiation.

Cytokine neutralization experiment. Washed platelets sourced identically were seeded into 96-well plates at a concentration of 1×10^8/mL. Each well then received neutralizing antibodies targeting RANTES (Biolegend, 515502, 1ug/mL), PF4 (Sino Biological, 10874-RP01, 1:300 dilution), and TGF-β (Biolegend, 146703, 13.5 μg/mL), with corresponding control groups established. Subsequently, the plate was incubated overnight in a CO_2-regulated incubator. The following day, the supernatant was collected; a portion was utilized for co-culture with Tn cells, while the remainder was collected and centrifuged at 3000 × *g* for 10 min, filtered with 0.22 μm filters, and stored at −80 °C for cytokine analysis. The isolation of unstimulated Tn cells was carried out as described in "Naïve CD4 T cell isolation," with four replicate wells established for each group. The collection of cells and preparation of samples for flow cytometry were conducted in accordance with the guidelines set forth in "Stimulation and cell staining" and "Flow cytometry analysis."

Detection of cytokines. Cytokines (RANTES and sCD40L) in cell culture supernatants and plasma were simultaneously measured using LEGENDplexTM customed assay kit (Biolegend, San Diego, USA) and the assay was performed in a V-bottom plate according to the manufacturer's protocol. Following incubation and wash steps, data acquisition was performed with BD FACSAria III (BD Biosciences) and analyzed using the LEGENDplexTM Data Analysis Software provided as an online cloud-based program (Biolegend). The sensitivity of the assay is provided in parentheses: RANTES (28.01 pg/mL) and sCD40L (11.27 pg/ mL).

Statistical analysis

Data are presented as mean ± standard error of the mean (SEM). Statistical analyses were conducted using GraphPad Prism 9 (GraphPad Software, San Diego, CA, USA) and R software (v4.2.1). For the assessment of differences between two matched groups, a paired *t*-test was employed. The comparison between two independent groups was performed using an unpaired Student's *t*-test or Mann–Whitney *U* test. For comparison of multiple groups, one-way analysis of variance (ANOVA) was used, followed by Tukey's honest significant difference post hoc test. These tests were followed by corresponding multiple comparisons tests. Correlation analysis was performed using Spearman's rank correlation. A p value of less than 0.05 was considered to indicate statistically significant.

Reporting summary

Further information on research design is available in the Nature Portfolio Reporting Summary linked to this article.

Data availability

The scRNA-seq data generated in this study have been deposited in the OMIX database under accession code OMIX006794 (https://ngdc.cncb.ac.cn/omix/select-edit/OMIX011097). Source data for the figures are provided with this paper. Access to the raw trial data is subject to controlled access due to legal and ethical restrictions related to participant privacy. Qualified researchers may request access by contacting the corresponding author. Requests will be evaluated by the institutional data access committee, and a response will be provided within 30 days. Access will be granted upon signing a data use agreement that limits the use of data to non-commercial, ethically approved research purposes only. Source data are provided with this paper.

References

1. Huijbers, M. G., Marx, A., Plomp, J. J., Le Panse, R. & Phillips, W. D. Advances in the understanding of disease mechanisms of autoimmune neuromuscular junction disorders. *Lancet Neurol.* **21**, 163–175 (2022).
2. Uzawa, A. et al. Roles of cytokines and T cells in the pathogenesis of myasthenia gravis. *Clin. Exp. Immunol.* **203**, 366–374 (2021).
3. Villegas, J. A., Van Wassenhove, J., Le Panse, R., Berrih-Aknin, S. & Dragin, N. An imbalance between regulatory T cells and T helper 17 cells in acetylcholine receptor-positive myasthenia gravis patients. *Ann. N. Y. Acad. Sci.* **1413**, 154–162 (2018).
4. Zhao, R., Luo, S. & Zhao, C. The role of innate immunity in myasthenia gravis. *Autoimmun. Rev.* **20**, 102800 (2021).
5. Payet, C. A. et al. Myasthenia gravis: an acquired interferonopathy? *Cells* **11**, 1218 (2022).
6. Scherlinger, M., Richez, C., Tsokos, G. C., Boilard, E. & Blanco, P. The role of platelets in immune-mediated inflammatory diseases. *Nat. Rev. Immunol.* **23**, 495–510 (2023).
7. Ribeiro, L. S., Migliari, B. L. & Franklin, B. S. Regulation of innate immune responses by platelets. *Front. Immunol.* **10**, 1320 (2019).
8. Maouia, A., Rebetz, J., Kapur, R. & Semple, J. W. The immune nature of platelets revisited. *Transfus. Med. Rev.* **34**, 209–220 (2020).
9. Koupenova, M., Clancy, L., Corkrey, H. A. & Freedman, J. E. Circulating platelets as mediators of immunity, inflammation, and thrombosis. *Circ. Res.* **122**, 337–351 (2018).
10. Semple, J. W., Italiano, J. J. & Freedman, J. Platelets and the immune continuum. *Nat. Rev. Immunol.* **11**, 264–274 (2011).
11. Li, N. CD4+ T cells in atherosclerosis: regulation by platelets. *Thromb. Haemost.* **109**, 980–990 (2013).
12. Spectre, G. et al. Platelets selectively enhance lymphocyte adhesion on subendothelial matrix under arterial flow conditions. *Thromb. Haemost.* **108**, 328–337 (2012).
13. Hu, H. et al. Platelets enhance lymphocyte adhesion and infiltration into arterial thrombus. *Thromb. Haemost.* **104**, 1184–1192 (2010).

14. Gerdes, N. et al. Platelets regulate CD4(+) T-cell differentiation via multiple chemokines in humans. *Thromb. Haemost.* **106**, 353–362 (2011).
15. Zhu, L., Huang, Z., Stalesen, R., Hansson, G. K. & Li, N. Platelets provoke distinct dynamics of immune responses by differentially regulating CD4+ T-cell proliferation. *J. Thromb. Haemost.* **12**, 1156–1165 (2014).
16. Smyth, S. S., Reis, E. D., Vaananen, H., Zhang, W. & Coller, B. S. Variable protection of beta 3-integrin-deficient mice from thrombosis initiated by different mechanisms. *Blood* **98**, 1055–1062 (2001).
17. Franks, Z. G., Campbell, R. A., Weyrich, A. S. & Rondina, M. T. Platelet-leukocyte interactions link inflammatory and thromboembolic events in ischemic stroke. *Ann. N. Y. Acad. Sci.* **1207**, 11–17 (2010).
18. Duffau, P. et al. Platelet CD154 potentiates interferon-alpha secretion by plasmacytoid dendritic cells in systemic lupus erythematosus. *Sci. Transl. Med.* **2**, 47ra63 (2010).
19. Zucoloto, A. Z. & Jenne, C. N. Platelet-neutrophil interplay: insights into neutrophil extracellular trap (NET)-driven coagulation in infection. *Front. Cardiovasc. Med.* **6**, 85 (2019).
20. Semeraro, F. et al. Extracellular histones promote thrombin generation through platelet-dependent mechanisms: involvement of platelet TLR2 and TLR4. *Blood* **118**, 1952–1961 (2011).
21. Huang, X. et al. The systemic inflammation markers as possible indices for predicting respiratory failure and outcome in patients with myasthenia gravis. *Ann. Clin. Transl. Neurol.* **10**, 98–110 (2022).
22. Gasparyan, A. Y., Ayvazyan, L., Mukanova, U., Yessirkepov, M. & Kitas, G. D. The platelet-to-lymphocyte ratio as an inflammatory marker in rheumatic diseases. *Ann. Lab. Med.* **39**, 345–357 (2019).
23. Jaretzki, A. R. et al. Myasthenia gravis: recommendations for clinical research standards. Task Force of the Medical Scientific Advisory Board of the Myasthenia Gravis Foundation of America. *Neurology* **55**, 16–23 (2000).
24. Linge, P., Fortin, P. R., Lood, C., Bengtsson, A. A. & Boilard, E. The non-haemostatic role of platelets in systemic lupus erythematosus. *Nat. Rev. Rheumatol.* **14**, 195–213 (2018).
25. Maugeri, N. et al. An intense and short-lasting burst of neutrophil activation differentiates early acute myocardial infarction from systemic inflammatory syndromes. *PLoS ONE* **7**, e39484 (2012).
26. Su, S. et al. VNTR2/VNTR3 genotype in the FCGRT gene is associated with reduced effectiveness of intravenous immunoglobulin in patients with myasthenia gravis. *Ther. Adv. Neurol. Disord.* **14**, 1279208315 (2021).
27. McDonald, B. et al. Platelets and neutrophil extracellular traps collaborate to promote intravascular coagulation during sepsis in mice. *Blood* **129**, 1357–1367 (2017).
28. Tan, S. et al. Platelets enhance CD4+ central memory T cell responses via platelet factor 4-dependent mitochondrial biogenesis and cell proliferation. *Platelets* **33**, 360–370 (2022).
29. Marcoux, G. et al. Platelet EVs contain an active proteasome involved in protein processing for antigen presentation via MHC-I molecules. *Blood* **138**, 2607–2620 (2021).
30. Tan, S. et al. Platelet factor 4 enhances CD4(+) T effector memory cell responses via Akt-PGC1alpha-TFAM signaling-mediated mitochondrial biogenesis. *J. Thromb. Haemost.* **18**, 2685–2700 (2020).
31. Patsouras, M. D. et al. Elevated expression of platelet-derived chemokines in patients with antiphospholipid syndrome. *J. Autoimmun.* **65**, 30–37 (2015).
32. Crawford, A., Angelosanto, J. M., Nadwodny, K. L., Blackburn, S. D. & Wherry, E. J. A role for the chemokine RANTES in regulating CD8 T cell responses during chronic viral infection. *PLOS Pathog.* **7**, e1002098 (2011).
33. De Wispelaere, K. & Freson, K. The analysis of the human megakaryocyte and platelet coding transcriptome in healthy and diseased subjects. *Int. J. Mol. Sci.* **23**, 7647 (2022).
34. Djaffar, I. et al. A new alternative transcript encodes a 60 kDa truncated form of integrin beta 3. *Biochem. J.* **300**, 69–74 (1994).
35. Schwertz, H. et al. Signal-dependent splicing of tissue factor pre-mRNA modulates the thrombogenicity of human platelets. *J. Exp. Med.* **203**, 2433–2440 (2006).
36. Nhek, S. et al. Activated platelets induce endothelial cell activation via an interleukin-1beta pathway in systemic lupus erythematosus. *Arterioscler. Thromb. Vasc. Biol.* **37**, 707–716 (2017).
37. Jin, W. et al. Single-cell RNA-Seq reveals transcriptional heterogeneity and immune subtypes associated with disease activity in human myasthenia gravis. *Cell Discov.* **7**, 85 (2021).
38. Gremmel, T., Frelinger, A. R. & Michelson, A. D. Platelet physiology. *Semin. Thromb. Hemost.* **42**, 191–204 (2016).
39. Delgado-Garcia, G. et al. Mean platelet volume is decreased in adults with active lupus disease. *Rev. Bras. Reumatol.* **56**, 504–508 (2016).
40. Turner-Stokes, L. et al. Measurement of haematological indices of chronic rheumatic disease with two newer generation automated systems, the H1 and H6000 (Technicon). *Ann. Rheum. Dis.* **50**, 583–587 (1991).
41. Matsumoto, K., Yasuoka, H., Yoshimoto, K., Suzuki, K. & Takeuchi, T. Platelet CXCL4 mediates neutrophil extracellular traps formation in ANCA-associated vasculitis. *Sci. Rep.* **11**, 222 (2021).
42. Colon, D. F. et al. Neutrophil extracellular traps (NETs) exacerbate severity of infant sepsis. *Crit. Care* **23**, 113 (2019).
43. Schechter, M. C. et al. Neutrophil extracellular trap (NET) levels in human plasma are associated with active TB. *PLoS ONE* **12**, e0182587 (2017).
44. Ceccarelli, F. et al. Assessment of disease activity in Systemic Lupus Erythematosus: lights and shadows. *Autoimmun. Rev.* **14**, 601–608 (2015).
45. Maugeri, N. et al. Platelet microparticles sustain autophagy-associated activation of neutrophils in systemic sclerosis. *Sci. Transl. Med.* **10**, eaao3089 (2018).
46. Pamuk, G. E. et al. Increased circulating platelet-neutrophil, platelet-monocyte complexes, and platelet activation in patients with ulcerative colitis: a comparative study. *Am. J. Hematol.* **81**, 753–759 (2006).
47. Kornerup, K. N., Salmon, G. P., Pitchford, S. C., Liu, W. L. & Page, C. P. Circulating platelet-neutrophil complexes are important for subsequent neutrophil activation and migration. *J. Appl. Physiol.* **109**, 758–767 (2010).
48. Panicker, S. R. et al. Circulating soluble P-selectin must dimerize to promote inflammation and coagulation in mice. *Blood* **130**, 181–191 (2017).
49. Schrottmaier, W. C., Kral, J. B., Badrnya, S. & Assinger, A. Aspirin and P2Y12 Inhibitors in platelet-mediated activation of neutrophils and monocytes. *Thromb. Haemost.* **114**, 478–489 (2015).
50. Hawwari, I. et al. Platelet transcription factors license the pro-inflammatory cytokine response of human monocytes. *EMBO Mol. Med.* **16**, 1901–1929 (2024).
51. Wienkamp, A. K., Erpenbeck, L. & Rossaint, J. Platelets in the NETworks interweaving inflammation and thrombosis. *Front. Immunol.* **13**, 953129 (2022).
52. Domer, D., Walther, T., Moller, S., Behnen, M. & Laskay, T. Neutrophil extracellular traps activate proinflammatory functions of human neutrophils. *Front. Immunol.* **12**, 636954 (2021).
53. Mandel, J., Casari, M., Stepanyan, M., Martyanov, A. & Deppermann, C. Beyond hemostasis: platelet innate immune interactions and thromboinflammation. *Int. J. Mol. Sci.* **23**, 3868 (2022).
54. McManus, C. M., Brosnan, C. F. & Berman, J. W. Cytokine induction of MIP-1 alpha and MIP-1 beta in human fetal microglia. *J. Immunol.* **160**, 1449–1455 (1998).
55. Wong, M. et al. Rantes activates Jak2 and Jak3 to regulate engagement of multiple signaling pathways in T cells. *J. Biol. Chem.* **276**, 11427–11431 (2001).

56. Colombara, M. et al. Constitutive activation of p38 and ERK1/2 MAPKs in epithelial cells of myasthenic thymus leads to IL-6 and RANTES overexpression: effects on survival and migration of peripheral T and B cells. *J. Immunol.* **175**, 7021–7028 (2005).
57. Lu, Y. et al. JAK2 inhibitor ameliorates the progression of experimental autoimmune myasthenia gravis and balances Th17/Treg cells via regulating the JAK2/STAT3-AKT/mTOR signaling pathway. *Int. Immunopharmacol.* **115**, 109693 (2023).
58. Sanders, D. B. et al. International consensus guidance for management of myasthenia gravis: executive summary. *Neurology* **87**, 419–425 (2016).
59. Zhu, H. et al. Human PBMC scRNA-seq-based aging clocks reveal ribosome to inflammation balance as a single-cell aging hallmark and super longevity. *Sci. Adv.* **9**, eabq7599 (2023).
60. Picelli, S. et al. Full-length RNA-seq from single cells using Smart-seq2. *Nat. Protoc.* **9**, 171–181 (2014).

Acknowledgements

This work was supported by the National Natural Science Foundation of China (Grant No. 62171299) and the National Key R&D Program of China, Precision Medicine Project (Grant No. 2017YFC0907700) awarded to Y.D. Additional support was provided to Q.W. by the Special Research Project of the National Clinical Key Specialty Construction Program (Grant No. 2024-ZZ-037). Special thanks are extended to Mingyang Wang, Liang Liu, Shiyue Hou, Xiyue Zhang, Junjie Wang, and the team at the National Center for Neurological Disorders of Xuanwu Hospital for their invaluable assistance in the laboratory. The authors also acknowledge the contribution of He Wang from the Ultra-Microstructure Analysis and Testing Center at Beijing Jiaotong University for his invaluable support in electron microscopy experiments.

Author contributions

Q.W., S.Z., Y.W., and H.L. contributed equally to this manuscript as co-first authors, performing the main experiments, analyzing experimental data, and drafting and revising the manuscript. J.W. and S.S. provided guidance on experimental design. Y.W. and N.X. conducted part of the in vivo experiments and analyzed the relevant data. Y.L., L.D., M.X., M.W., H.C., and S.W. participated in the study design. W.Z. and X.W. were responsible for the bioinformatic analysis. D.W., S.Z., W.L., and Z.T. contributed to the flow cytometry conduction. J.D. and Y.H. were involved in the sample collection. Jinming H., G.C., and R.D. contributed to the study design and manuscript revision. Y.D., Junwei H., and X.L. contributed equally as corresponding authors, providing essential instructions, supervising the experiments, and revising the manuscript. All authors read and approved the final manuscript.

Competing interests

The authors declare no competing interests.

Additional information

Supplementary information The online version contains supplementary material available at https://doi.org/10.1038/s41467-025-63750-2.

Correspondence and requests for materials should be addressed to Xiaoli Li, Junwei Hao or Yuwei Da.

Peer review information *Nature Communications* thanks Silvia Falso, Maartje Huijbers, John Hwa, and the other, anonymous, reviewer(s) for their contribution to the peer review of this work. A peer review file is available.